COMPENDIUM OF MEASURED RHEO-OPTICAL PROPERTIES OF HYSOL 4485

Ker C. Thomson, Editor

TRUSTEES OF BOSTON COLLEGE
Chestnut Hill, Mass. 02167

Contract AF19(628)-212

Scientific Report No. 1

March 1965

Project 8652

Task 865205

Prepared for

AIR FORCE CAMBRIDGE RESEARCH LABORATORIES
OFFICE OF AEROSPACE RESEARCH
UNITED STATES AIR FORCE
BEDFORD, MASSACHUSETTS

WORK SPONSORED BY ADVANCED RESEARCH PROJECTS AGENCY

PROJECT VELA-UNIFORM

ARPA ORDER NO. 292

Project Code No. 8100 Task 2

Requests for additional copies by Agencies of the Department of Defense, their contractors, and other government agencies should be directed to the:

Defense Documentation Center
Cameron Station
Alexandria, Virginia 22314

Department of Defense contractors must be established for DDC services, or have their 'need-to-know' certified by the cognizant military agency of their project or contract.

All other persons and organizations should apply to the:

Clearinghouse for Federal Scientific and
Technical Information (CFSTI)
Sills Building
5185 Port Royal Road
Springfield, Virginia 22151

COMPENDIUM OF MEASURED RHEO-OPTICAL PROPERTIES OF HYSOL 4485

Ker C. Thomson, Editor

TRUSTEES OF BOSTON COLLEGE
Chestnut Hill, Mass. 02167

Contract AF19(628)-212

Scientific Report No. 1

March 1965

Project 8652

Task 865205

Prepared for

AIR FORCE CAMBRIDGE RESEARCH LABORATORIES
OFFICE OF AEROSPACE RESEARCH
UNITED STATES AIR FORCE
BEDFORD, MASSACHUSETTS

WORK SPONSORED BY ADVANCED RESEARCH PROJECTS AGENCY

PROJECT VELA-UNIFORM

ARPA ORDER NO. 292

Project Code No. 8100 Task 2

ABSTRACT

A measuring program was conducted with the aim of determining the complete rheo-optical characterization of a certain urethane rubber compound (HYSOL 4485) suitable for dynamic photo-viscoelastic studies. The shift curve and the master curve at 60°F are presented for both the Shear Storage Modulus and the Shear Loss Tangent. In determining the shear properties sinusoidal loading of specimens cut as hollow cylinders was used. Using a method designed originally by Selway and Brown the dynamic stress optic coefficient and the complex Youngs Modulus were measured at room temperature. The following tests were conducted in an atmosphere maintained at 70°F and 40% R.H. Youngs Modulus in creep was measured at two stress levels: 20.0 and 41.7 p.s.i. Dynamic stress-strain curves were determined using Volterra pendulum tests at two initial velocities 7.02 and 65.5 inches per second; and the static and dynamic stress optic coefficients were measured.

CONTENTS

LIST OF FIGURES

LIST OF FIGURES (Cont'd)

LIST OF FIGURES (Cont'd)

LIST OF TABLES

INTRODUCTION

At Cambridge Research Laboratories an optical technique for following stress wave propagation in large transparent sheets has been developed. The apparatus used is similar to the stroboelastic equipment developed by Becker (1) (see also Thomson (2). It differs from his in using models increased in size by an order of magnitude and with the time length of the source function shortened so that the spacial length of the wave packet produced is less than the smallest dimension of the model and propagation of the entire wave can be observed, as discussed in Thomson and Hill (3). Behind this interest lies the hope that the technique can be used to model seismic problems of interest. It offers the advantage over conventional electronic transducer techniques that not only is the action viewed at particular points as a function of time it is also viewed throughout all of space and time wherever the wave packet exists. With a continuously variable phase relationship between striking and flashing the operator is able to study the wave as it propagates and then "lock" on the viewing screen any particular phase of the action of special interest and photograph it. Before the technique can be "tailored" to fit particular problems in seismology it is necessary (in most cases) to have quantitative knowledge of the physical properties of both the prototype and the model. This compendium is concerned with the latter problem only.

The properties which are of interest for a particular material are the stress and strain optic coefficients, and any two elastic moduli. Earth materials show properties which are strain rate dependent so the coefficients and moduli mentioned above should actually be measured as functions of frequency or time. Another requirement on materials for optical modelling by means of the repetitive technique is extreme optical sensitivity and low modulus. The high optical sensitivity is required to enable the stress in the model to be quantitatively measured at points where it has dropped to low levels. Low modulus is an advantage as it implies low wave speed and hence less blurring of the isochromatic fringes as they propagate under stroboscopic illumination. Unfortunately most materials which have these characteristics are also temperature sensitive. It is desirable then to measure the stress optic coefficient, strain optic coefficient and a pair of elastic moduli as function of both frequency and temperature.

On reference to the literature one suitable material would appear to be HYSOL 4485. This is a Urethane rubber compound identified as HYSOL 8705 in older papers published prior to the product number change by the Hysol Corporation. The manufacturers specifications indicate high optical sensitivity, low elastic modulus and availability in convenient sheets, thus eliminating the user casting operations associated with many other similar products. In addition strain rate dependent physical properties had been measured for this material in previous studies. This

suggested viscoelasticity which was of particular interest, because one of the first seismic modelling problems proposed for the optical modelling technique was Lamb's two dimensional problem for a visco-elastic half space.

A considerable volume of literature exists on the visco-elastic properties of this material. However, on consideration of these published observations, and the assumptions inherent in making them and reducing the results, and the use to which the data was to be put, it became apparent that some inadequacies existed. Previous experimenters have measured Youngs Modulus (in creep, relaxation, at constant strain rate, sinusoidally or with ballistic pendula techniques) and have <u>assumed incompressibility</u> (i.e., infinite bulk modulus or Poissons ratio about 1/2) in order to complete the presentation of the two functions required for entire specification of the mechanical properties of any linearly visco-elastic isotropic material. Attempts to estimate Poissons ratio from published data suggested that this ratio was close to 1/2 at very low (creep) frequencies, but that at higher frequencies it might drop to much lower values in possible violation of the assumptions usually made about it. In order to provide further experimental information for specifying the somewhat elusive physical properties of this material, the measuring program outlined in the following pages was undertaken.

Catholic University of America measured the shear modulus as a function of temperature and frequency by means of dynamic torsional equipment enclosed in an environmental chamber. The University of California Institute of Engineering Research measured the dynamic elastic modulus and dynamic stress optic coefficient as functions of frequency. Armour Research Foundation performed creep tests at two stress steps, Volterra pendulum tests at two initial velocities, and measured the static stress optic coefficient, the complex Youngs Modulus and the complex shear modulus in the frequency interval 100-700 c.p.s. Armour's measurements were all conducted at 70°F and 40% relative humidity.

All of the tasks described in this compendium were performed as subcontracts under Air Force Contract AF19(628)-212 with Boston College, Chestnut Hill, Mass.

MEASUREMENT OF THE DYNAMIC SHEAR MODULUS OF HYSOL 4485 AS A FUNCTION OF FREQUENCY AND TEMPERATURE

This report presents the results of the measurement of the shear storage modulus G' and shear loss tangent G"/G' of HYSOL 4485 supplied by Weston Observatory, Weston, Mass.

A detailed description of the experimental system and data reduction technique is included in Reference (4). We shall report herein recent improvements in the experimental system and the results of these particular measurements, including length studies and error analysis. The test is based on the torsional oscillations of a circular cylindrical sample of finite length. For these particular tests the specimen was hollow with dimensions of 1.000 inches outside diameter, 0.500 inches inside diameter by 0.500 inches in length. The measurements reported herein are the results of three runs at selected temperatures. The data reduction procedure is described in detail in Reference (4) wherein there is a Fortran listing of the data reduction computer program.

The results of the measurements are shown in Figs. 1(a) through 1(i), inclusive. Raw data collected at 12 deg. F.,

20 deg. F., 26 deg. F., 26 deg. F., 30 deg. F., 35 deg. F., 40 deg. F., 48 deg. F., 60 deg. F., and 70 deg. F. are shown in Figs. 1. The data were plotted and the average curves representing the amplitude and phase responses were passed through the data points as shown. The data for the data reduction procedure were obtained from these average curves. The reduced data for the shear modulus are shown in Fig. 2.

Among all materials that satisfy approximately linear visco-elastic laws at uniform temperature are a group which exhibit a particularly simple property with change of temperature. This is a translational shift - no change in shape - of the shear storage modulus plotted against the logarithm of frequency at different uniform temperatures. This property leads to an equivalence relation between temperature and the $\log_{10}$ of frequency which was originally proposed by Leadermann (5) and which has been called the time-temperature shifting principle. This same postulate was introduced in a slightly different form by Ferry (6) and materials exhibiting such behavior have been termed "thermorheologically simple" by Schwarzl and Staverman (7). The postulate has been confirmed experimentally for a variety of visco-elastic materials. It was first applied to experimental data in an explicit numerical fashion by Tobolsky and his co-workers (8). They introduced a shift function and modified the

shifting principle to account for the proportionality of the modulus to absolute temperature. Thus, the analytical statement of the time-temperature shifting principle is given by

$$\frac{1}{T} G'_T(f) \quad - \quad \frac{1}{T_o} G'_{T_o}(\xi)$$

wherein f denotes the frequency, T and T_o two different absolute temperatures, G'_T and G'_{T_o} the shear storage modulus at the two different absolute temperatures in question and denotes the 'reduced frequency' given by

$$\xi = f\, a_T$$

The shift factor a_T is defined in terms of a shift function F(T) by means of

$$F(T) = \log_{10} a_T$$

The shift function F(T) at the absolute temperature T is the actual amount of shifting required parallel to the $\log_{10} f$ axis in order to superimpose the data collected at the absolute temperature T upon that collected at a reference absolute temperature T_o.

In order to test whether or not the HYSOL 4485 sample under investigation belongs to the class of thermorheologically simple

materials and in order to extend the frequency range of the measurements, the shifting principle was applied to the shear storage modulus data of Fig. 2. The master curve of Fig. 3 is the result. The reference temperature selected was 60 deg. F. and the shift factor a_T required is plotted as a function of temperature in Fig. 4.

Using this same shift factor, the master curve for the shear loss tangent was constructed with the result shown in Fig. 5. In this case the procedure was somewhat different. The data reduction procedure yields the shear loss modulus G'' as well as the shear storage modulus G'. Their ratio constitutes the shear loss tangent.

It is clear that the HYSOL 4485 sample is, indeed, therm-rheologically simple. Therefore, we have, in effect, extended the frequency range over which the measurements were made.

A hollow cylindrical sample of HYSOL 4485 was cast. The cast sample had dimensions of 1.000 inches outside diameter and 0.500 inches inside diameter by 2.000 inches long. The sample was bonded to two sample holders and tested. The sample was then reduced in length to 1.500 inches and again tested. This procedure was repeated for lengths of 1.000 and 0.500. The results of this test is shown in Fig. 6, wherein the shear storage modulus G', is plotted for the lengths under investigation.

DATA ACQUISITION SYSTEM

The function of the data acquisition system is to measure the accelerations of the input and output bell-cranks and the phase angle between these accelerations together with the frequency of the applied harmonic oscillations. In order to accomplish this purpose piezo-electric crystal accelerometers are mounted on the two bell-cranks using electrically insulated studs. The analog voltages are then impedance matched and amplified, with a gain of ten, using a cathode follower circuit with an integrated amplifier. The amplified voltages are used with the automatic vibration exciter for frequency sweeping with automatic level control. During the frequency sweep, the signal from the input accelerometer is used with the vibration exciter as a control voltage.

The analog signal from the output accelerometer is recorded with a Level Recorder using True RMS detection. The frequency calibrated axis of the Level Recorder can be syncronized with the frequency of the oscillator thus offering exact amplitude-frequency identification. This amplification ratio versus frequency plot is used to establish the general nature of the frequency response. Such information is extremely valuable during actual testing.

The analog voltages from the two accelerometers are alternately measured using a frequency analyzer with True RMS detection.

The frequency of the 6% filter in the analyzer is set using the frequency determined from the previous frequency count. Filtering minimizes extraneous harmonics and cable noise while using the same analyzer for the two different signals reduces calibration difficulties.

True RMS detection is used in order to minimize the effect of perturbations of the signal caused by extraneous noise.

At all data points the feedback circuit in the selective amplifier section of the Frequency Analyzer is switched so it is rearranged, such that the Analyzer functions as a frequency rejection amplifier. When set as a frequency rejection amplifier any frequency in the test range can be attenuated by at least 60 db. With this operation a distortion and noise measurement is obtained. The smallest signal-to-noise ratio acceptable in this experiemtnt is 30 db. thus assuring a minimum of error, due to noise, as shown in Fig.

In measuring the phase angle between the two accelerometer signals we must be careful to account for any phase shifts that are introduced into the system by the electronic circuitry. We can avoid the difficulties in such an accounting by assuring that the phase shifts are the same in the individual accelerometer read-out circuits. This function is accomplished by the phase compensating circuit shown in Fig. 8(b). The voltage level of an

AC signal from the oscillator section of the automatic vibration exciter control is reduced to the same voltage level as the amplified accelerometer signals. This standard signal is divided and passed through the individual legs of the accelerometer read-out circuitry which is ultimately used in data acquisition. The phase angle between the signals in the two legs is measured in a counter. In general, this phase angle will not be zero because of phase shifts introduced by the electronic elements in each leg. Now, one of the variable filters is adjusted so that the phase angle is zero, thus assuring that the phase shifts in the two read-out circuits are identical.

Now, the standard signal from the oscillator is replaced by the actual amplified accelerometer signals as shown in Fig. 8(c).

The gain of one or the other of the No. 2 amplifiers is adjusted with an input potentiometer. Equalization is needed because the counter is amplitude sensitive. Clearly, this gain adjustment does not affect the phase relationship. The time interval between corresponding points on the two sine waves is then measured. Triggering circuitry is provided in the counter previously used for measuring frequency. This circuitry is voltage dependent, and it is for this reason that the amplitude of the two accelerometer signals is equalized. It is clear that the individual instruments in the phase measuring circuits can only

introduce error into the phase angle measurement by harmonic distortion and not by their gain or attenuation as the amplitude of the two accelerometer signals have been equalized.

For convenience in the calculation of phase angle the counter is now switched to trigger at the same amplitude on succeeding sine waves of the same signal. The measured period together with the measured time interval is used to calculate the phase angle between the accelerometer signals.

ANALYSIS OF ERROR IN DATA ACQUISITION SYSTEM

The vibration control sub-system includes three main items of equipment: an oscillator, a power control amplifier and two electromagnetic vibrators. Since these three items are not used directly in the determination of phase or amplitude measurement we need only concern ourselves with harmonic distortion and vibrator resonance. Harmonic distortion of the oscillator and amplifier combination is 0.26% in the 20-2,000 cps range at maximum power output. The first resonance of the electromagnetic vibrator is 3875 cps, well beyond the 2,000 cps upper limit of the investigation.

In this test we are only interested in relative movements, the acceleration ratio between the upper and lower bell-cranks, thus an absolute acceleration is not needed. A back-to-back

calibration is performed on the two read-out accelerometers throughout the frequency range under investigation prior to performing each test. Such a test has found the accelerometers to have a frequency response of ±1/2% in the 20-2000 cps range and a phase shift of such small magnitude that it cannot be read with a 6-digit counter. Linearity studies have found the accelerometers to have a linearity of ±1% throughout the frequency range of the test.

The cathode follower and integrated amplifier have a distortion of 0.49%, linearity of 2.5% and phase shift between channel of less than 1^{o} throughout the test frequency range.

Since both legs of the phase measuring network are amplitude equalized we need only concern ourselves with the harmonic distortion of each element. Harmonic distortion of the amplifiers has been found to be 0.1%. Harmonic distortion of the filters has been found to be 0.68%.

The accuracy of the counter, both in frequency and time interval measurement is 1 part in 1000.

The single voltmeter used for measuring the amplitude of the two accelerometer signals has an accuracy of 0.1%.

The specific equipment used in the data acquisition system is described in Table 1.

FIG. 1 a

AMPLITUDE AND PHASE RESPONSE
OF HYSOL 4485 AT 12° F.

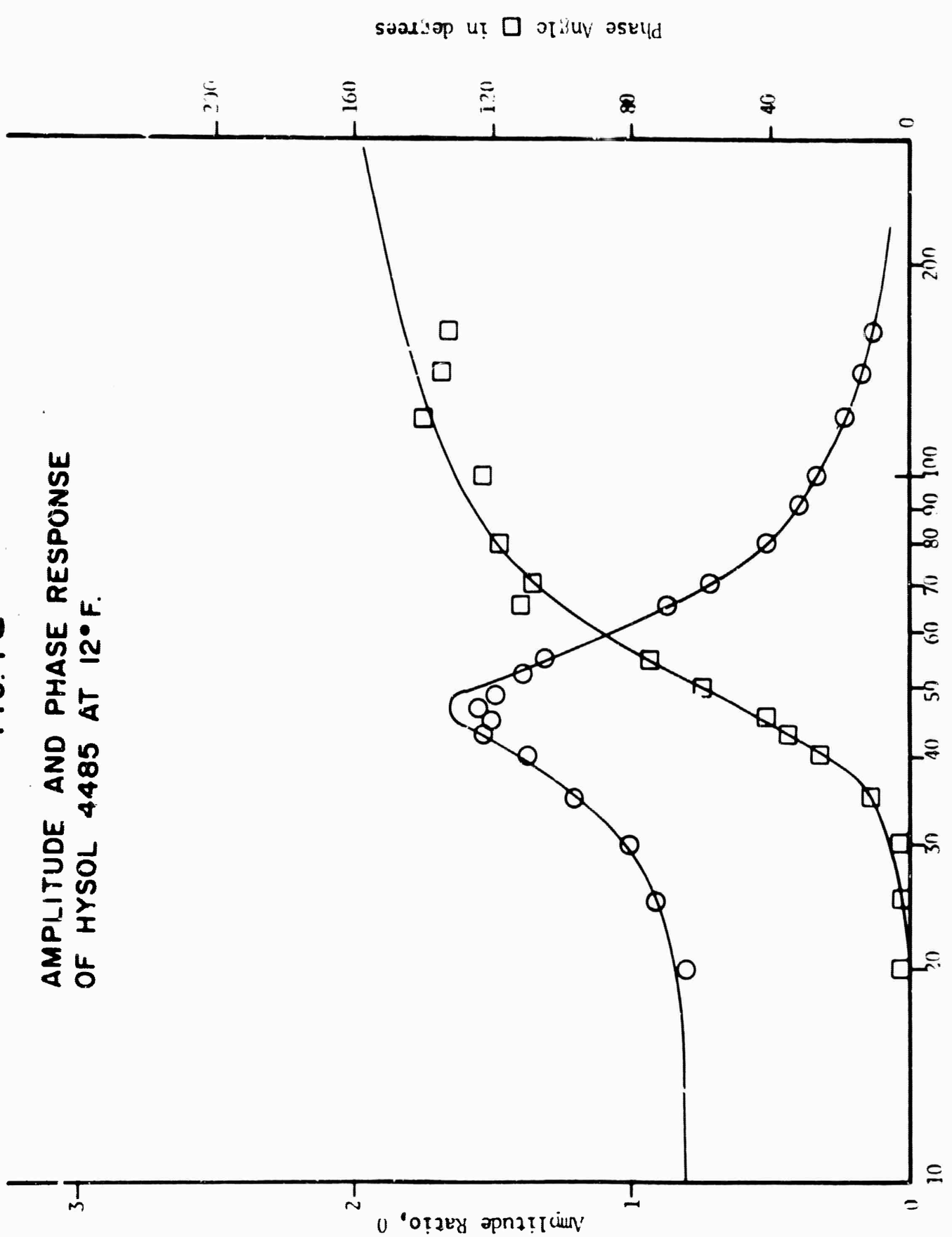

FIG. 1 b

FIG. 1b

AMPLITUDE AND PHASE RESPONSE
OF HYSOL 4485 AT 20° F.

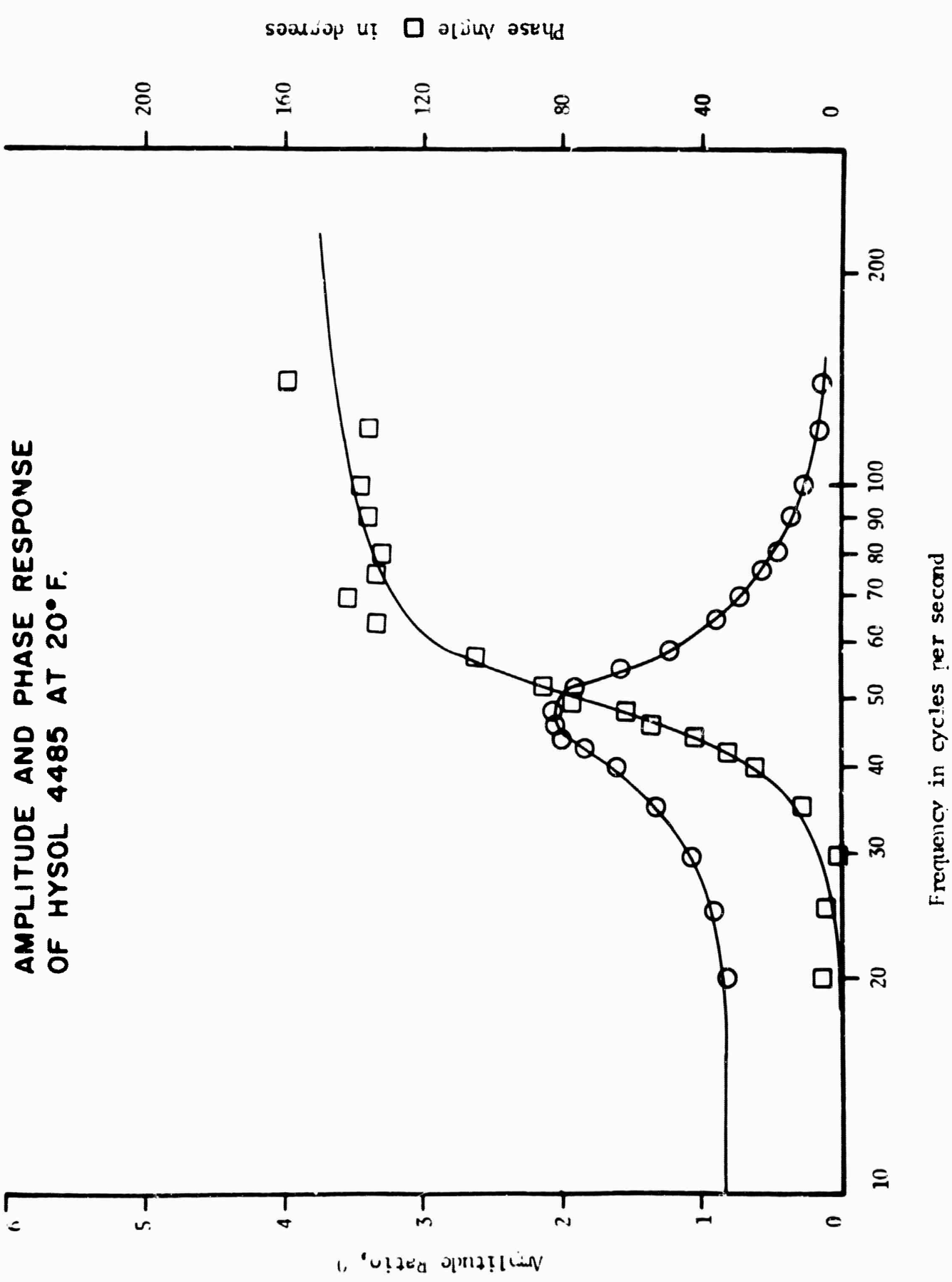

FIG. 1c

AMPLITUDE AND PHASE RESPONSE
OF HYSOL 4485 AT 26° F.

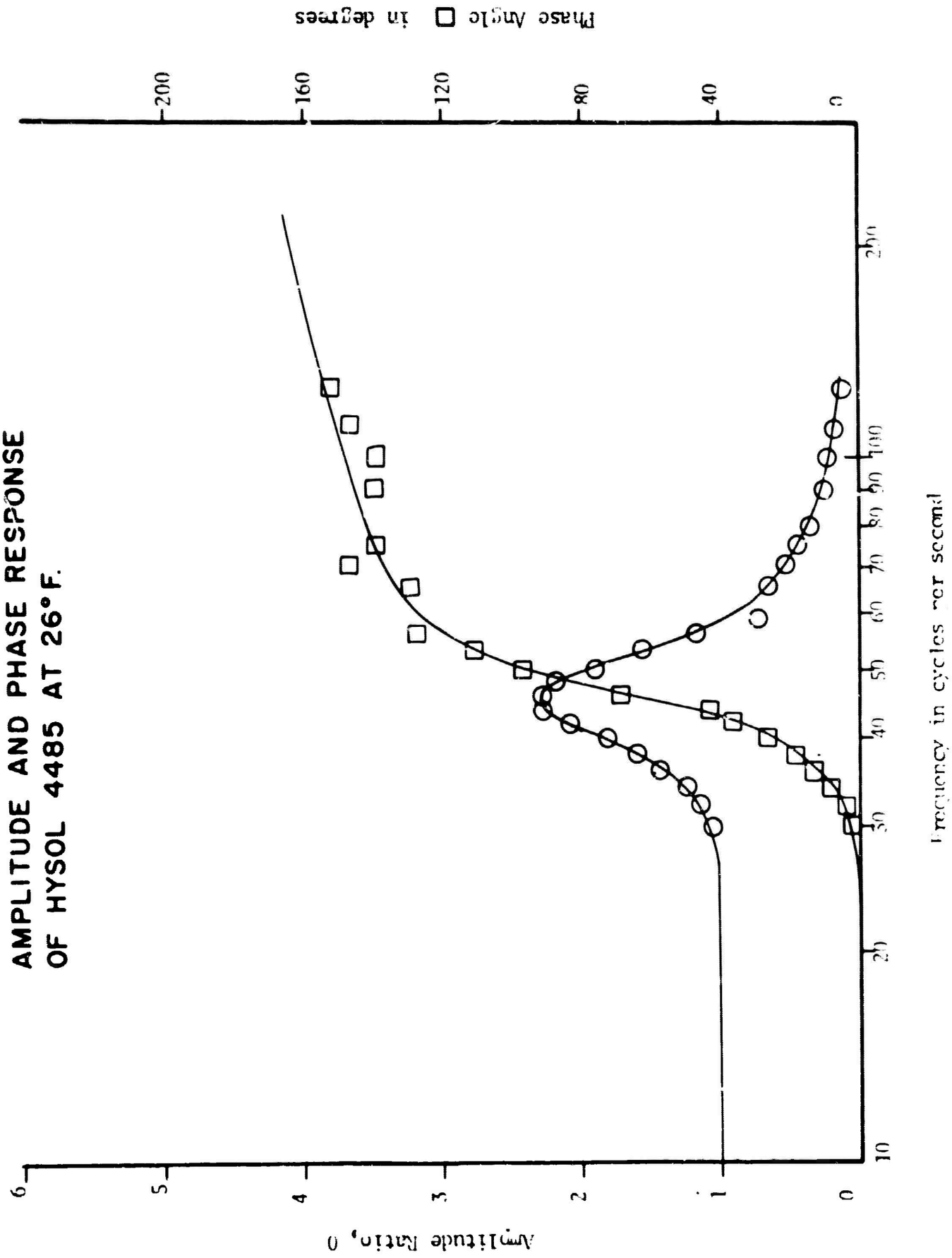

FIG. 1 d

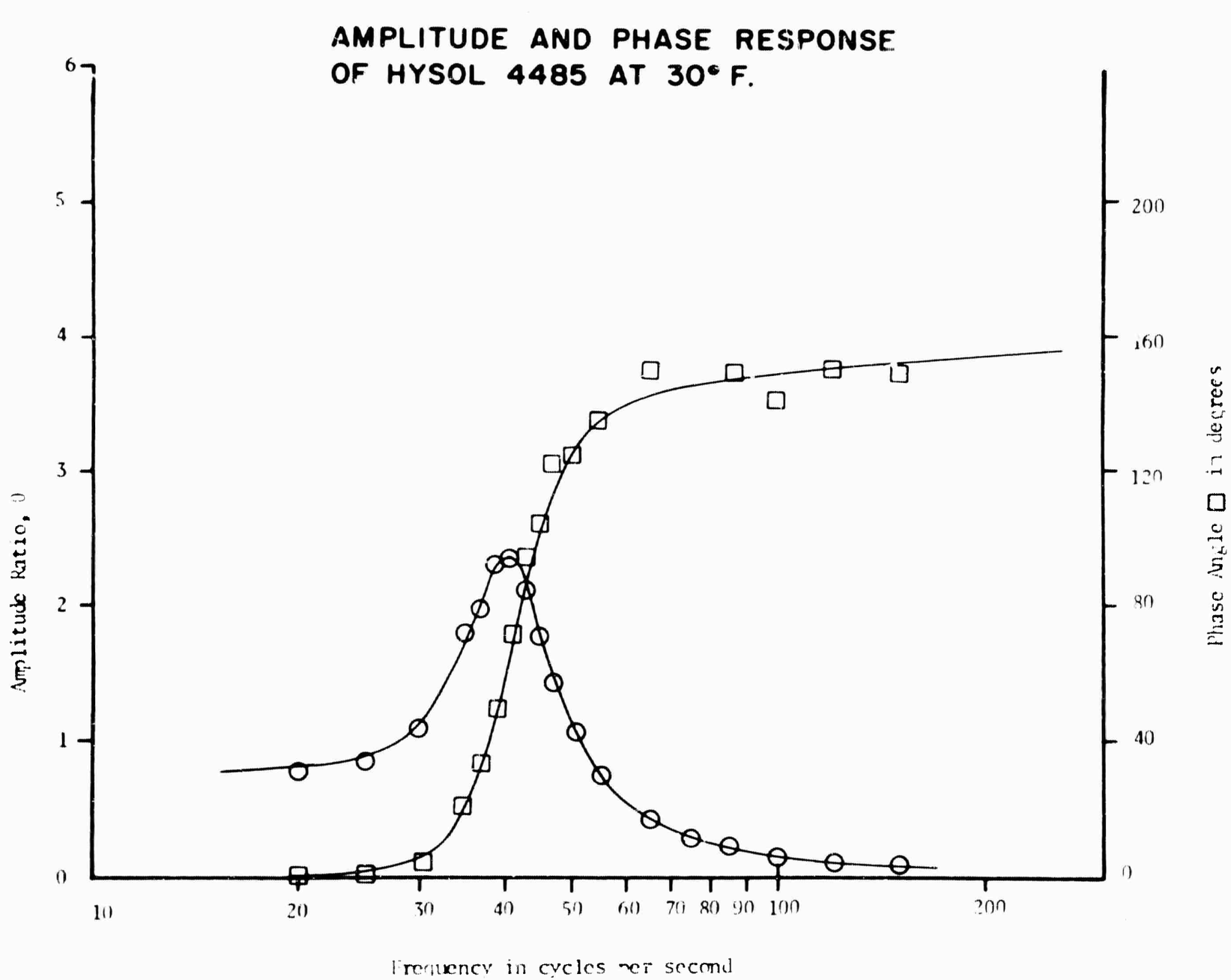

FIG. 1 e

AMPLITUDE AND PHASE RESPONSE
OF HYSOL 4485 AT 35° F.

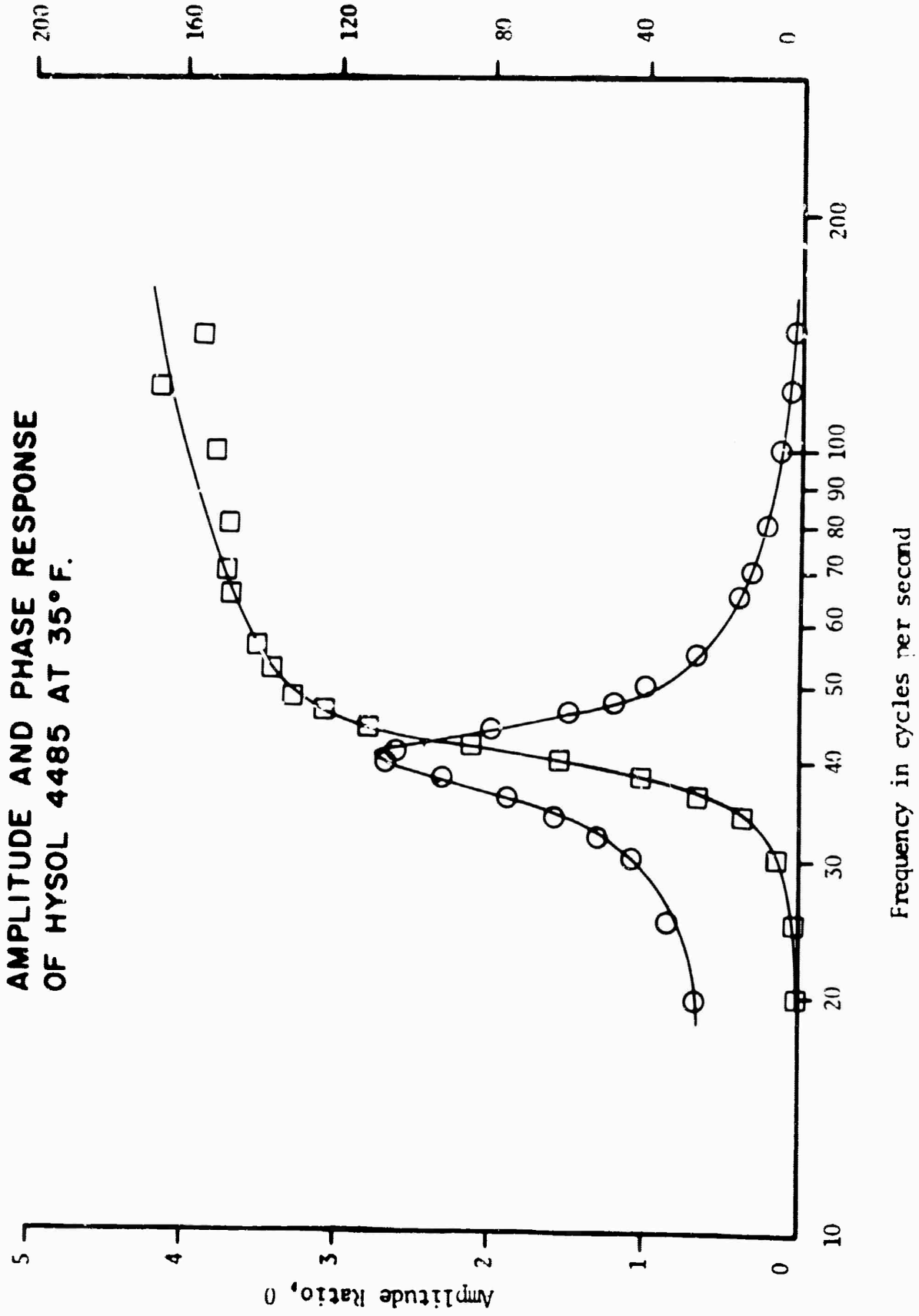

FIG. 1 f

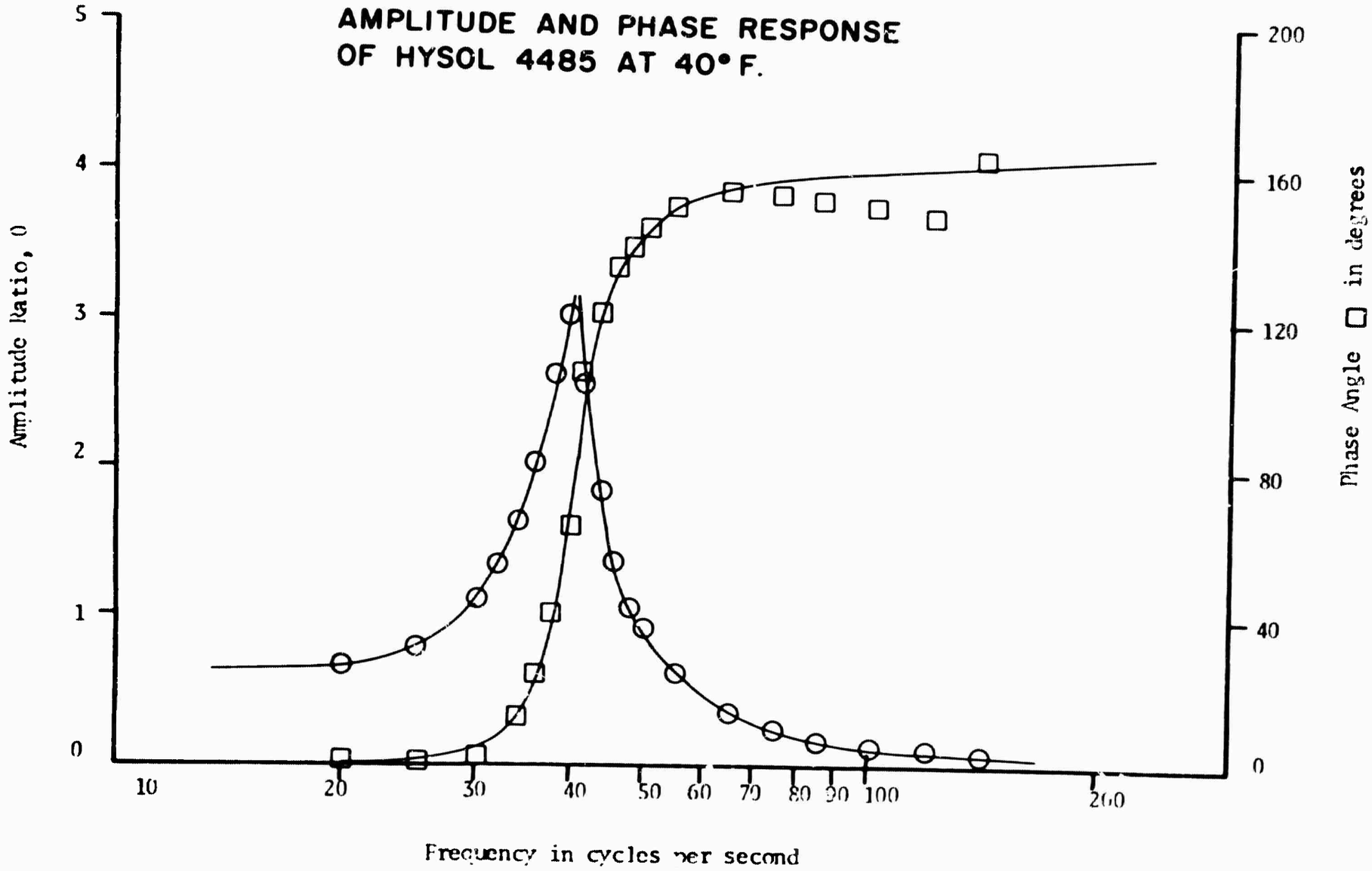

FIG. 1g

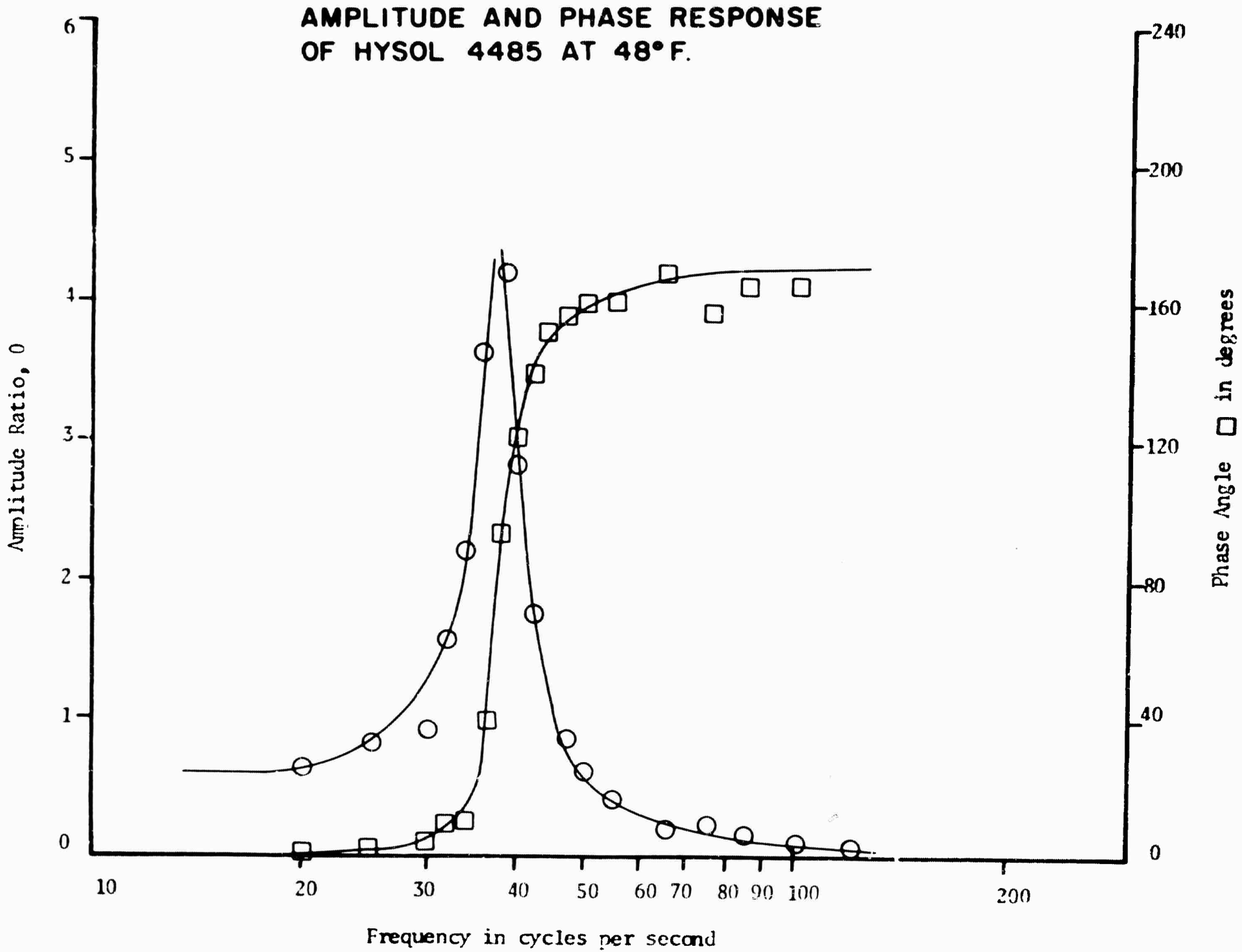

FIG. 1 h

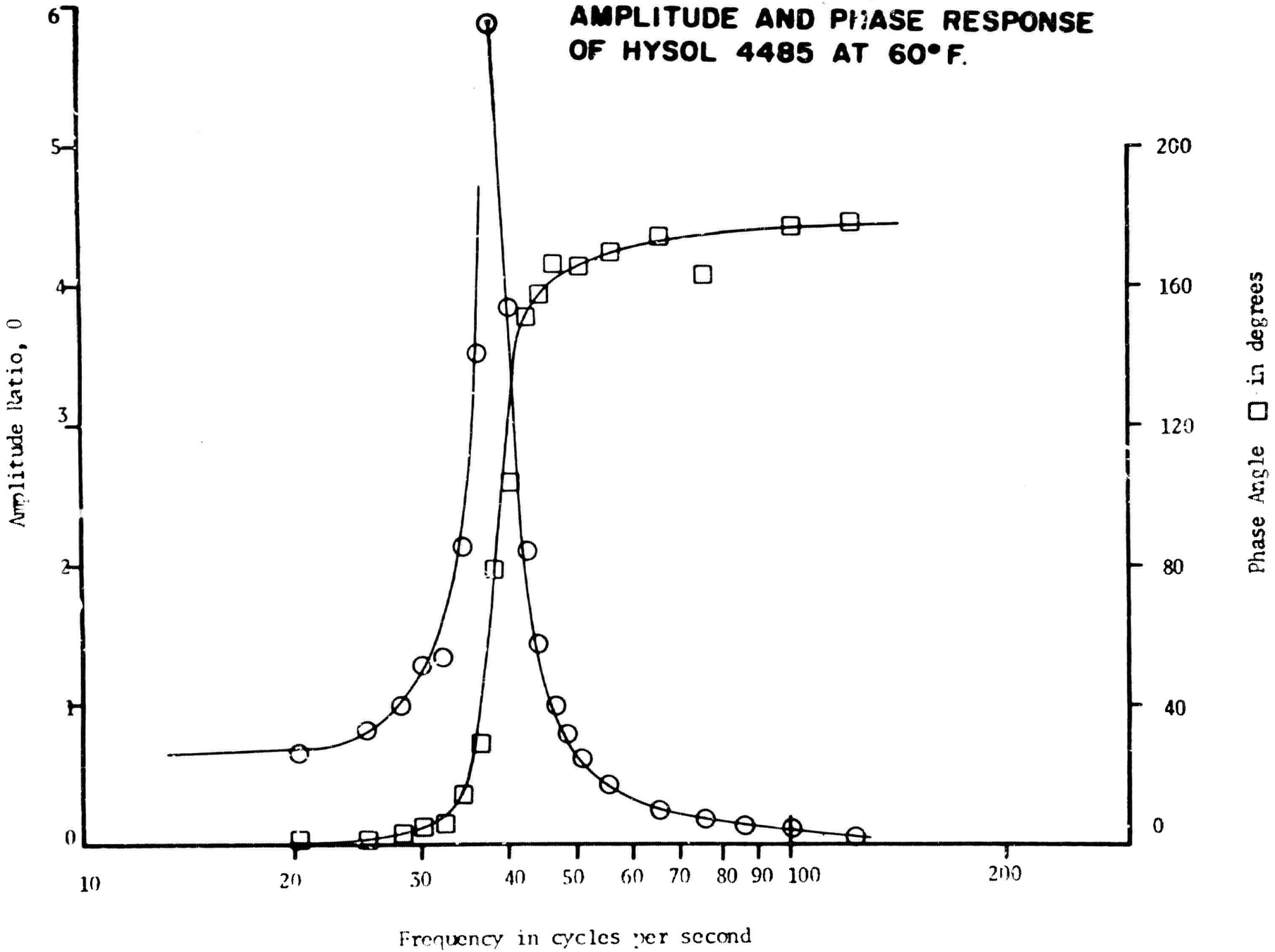

FIG. 1 i

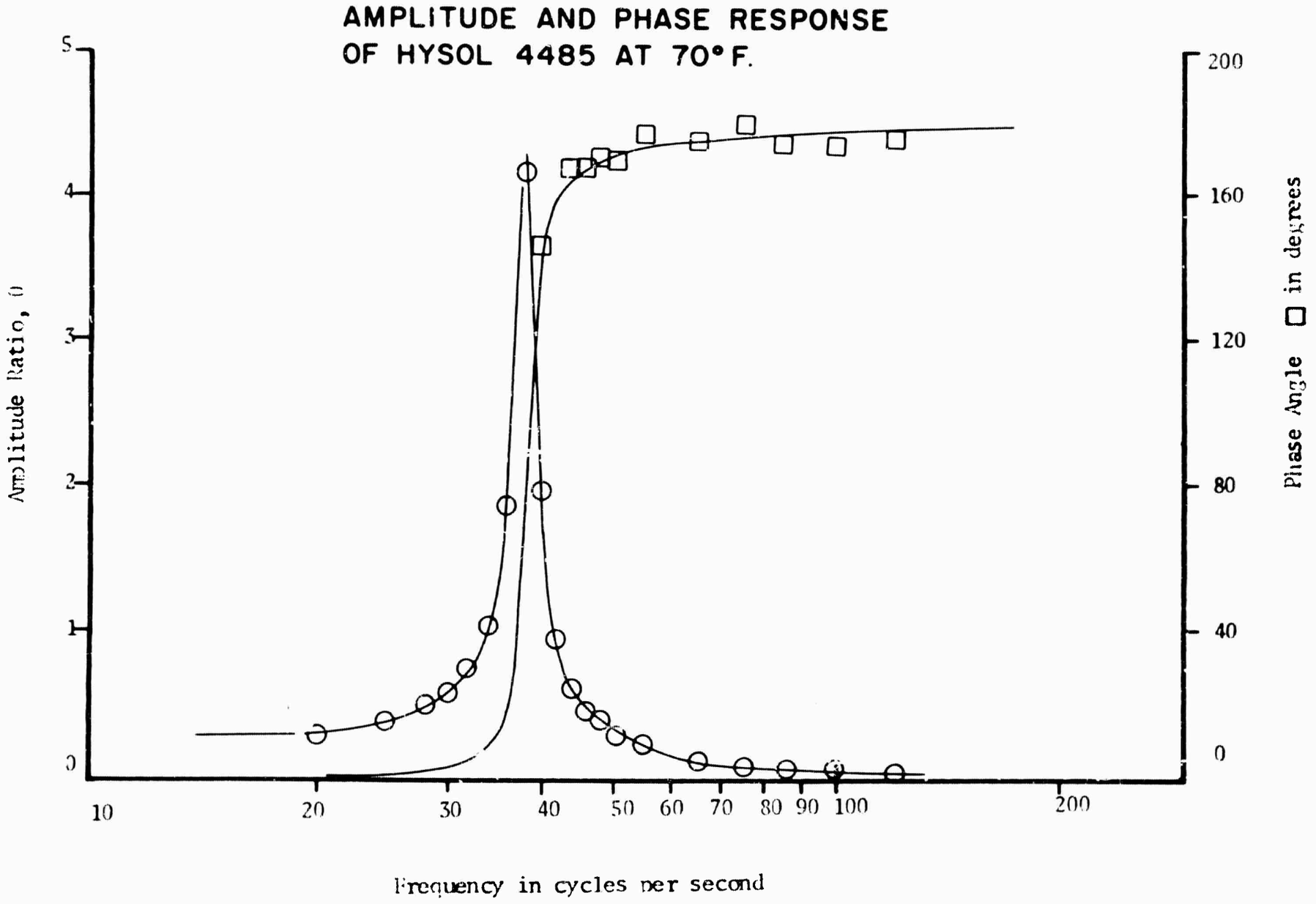

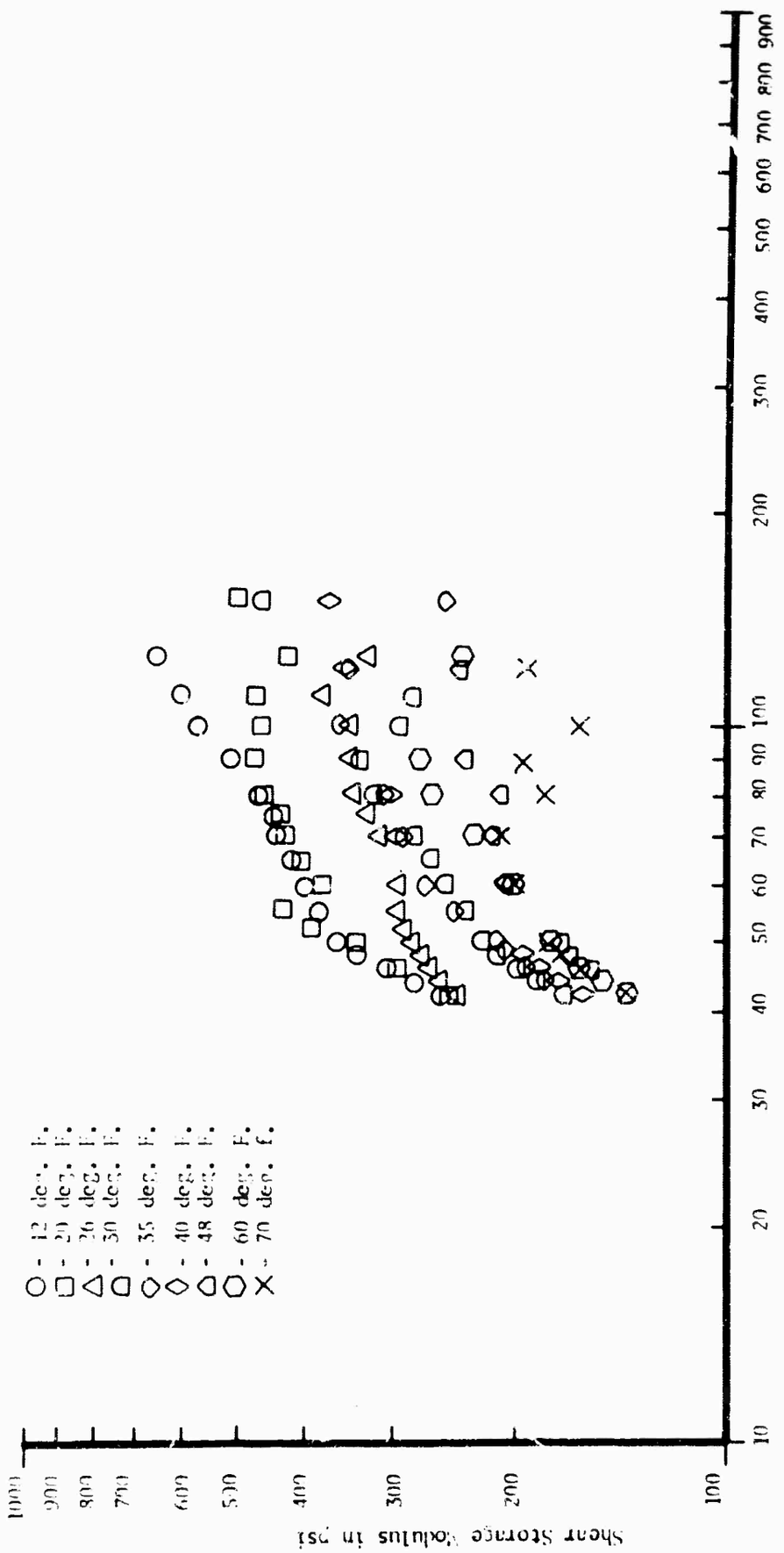

FIG. 2 SHEAR STORAGE MODULUS VS. FREQUENCY FOR HYSOL 4485.

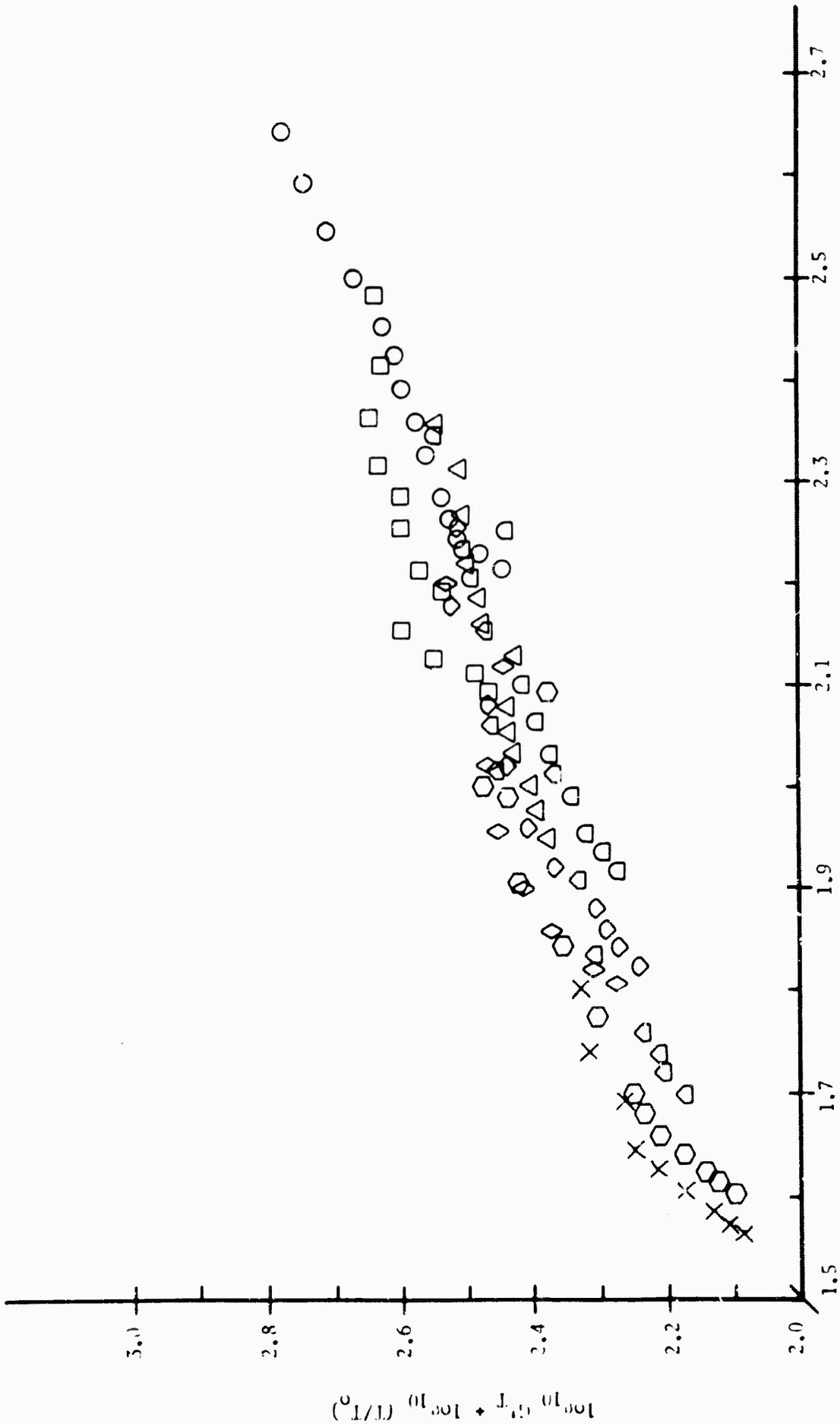

FIG. 3 MASTER CURVE FOR SHEAR STORAGE MODULUS OF HYSOL 4485.

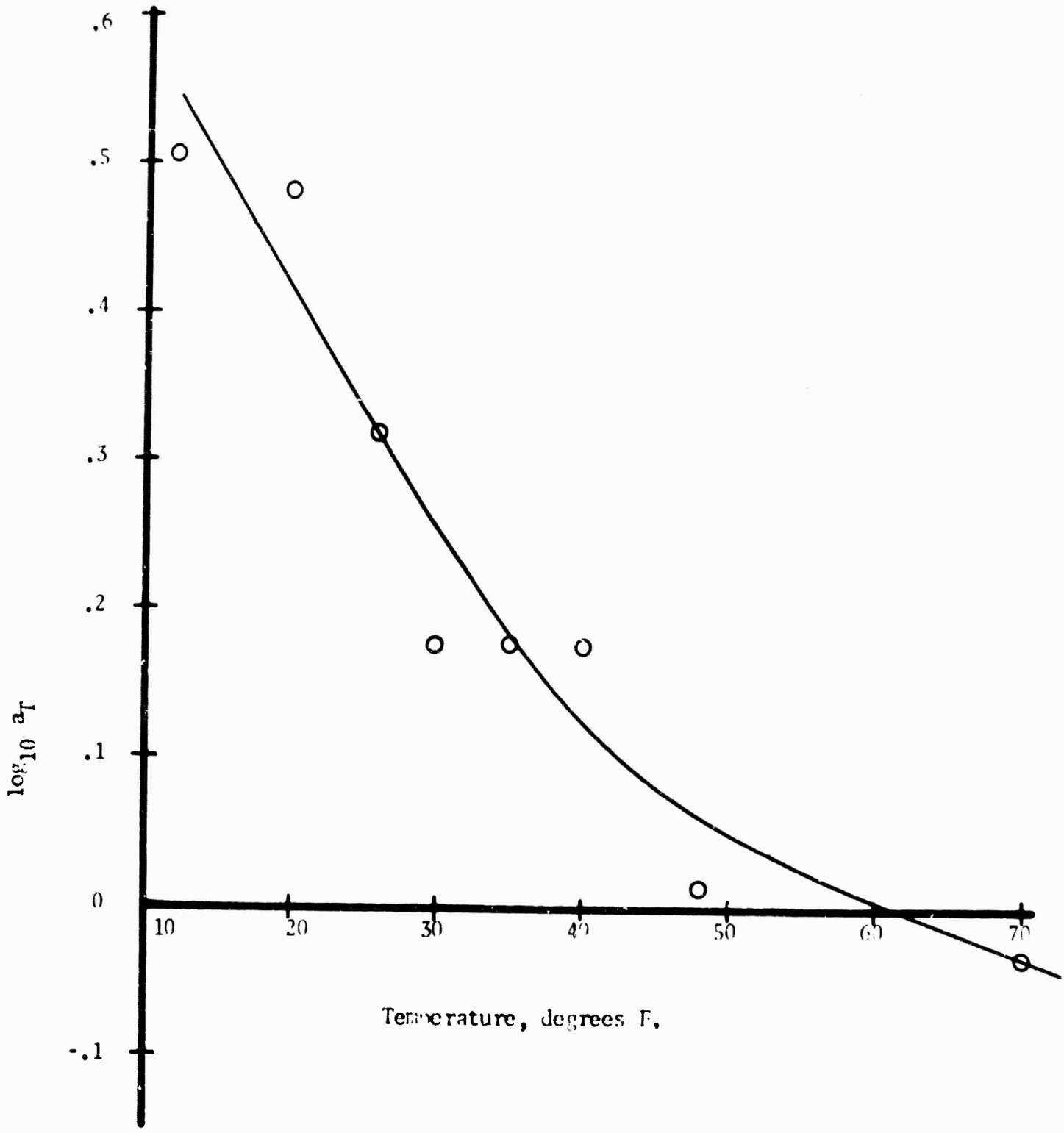

FIG. 4 SHIFT FACTOR AS A FUNCTION OF TEMPERATURE FOR HYSOL 4485.

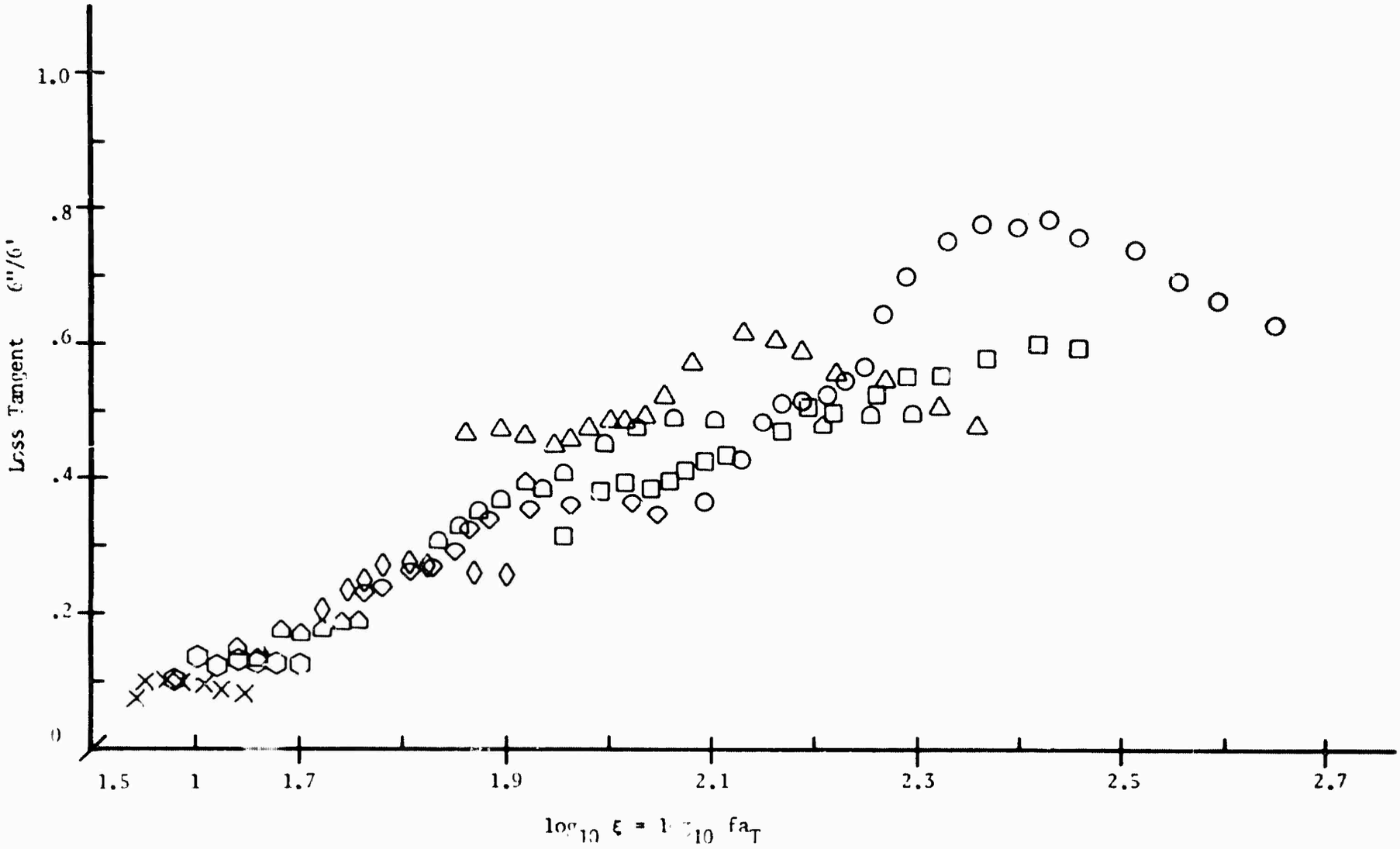

FIG. 5 MASTER CURVE FOR SHEAR LOSS TANGENT OF HYSOL 4485.

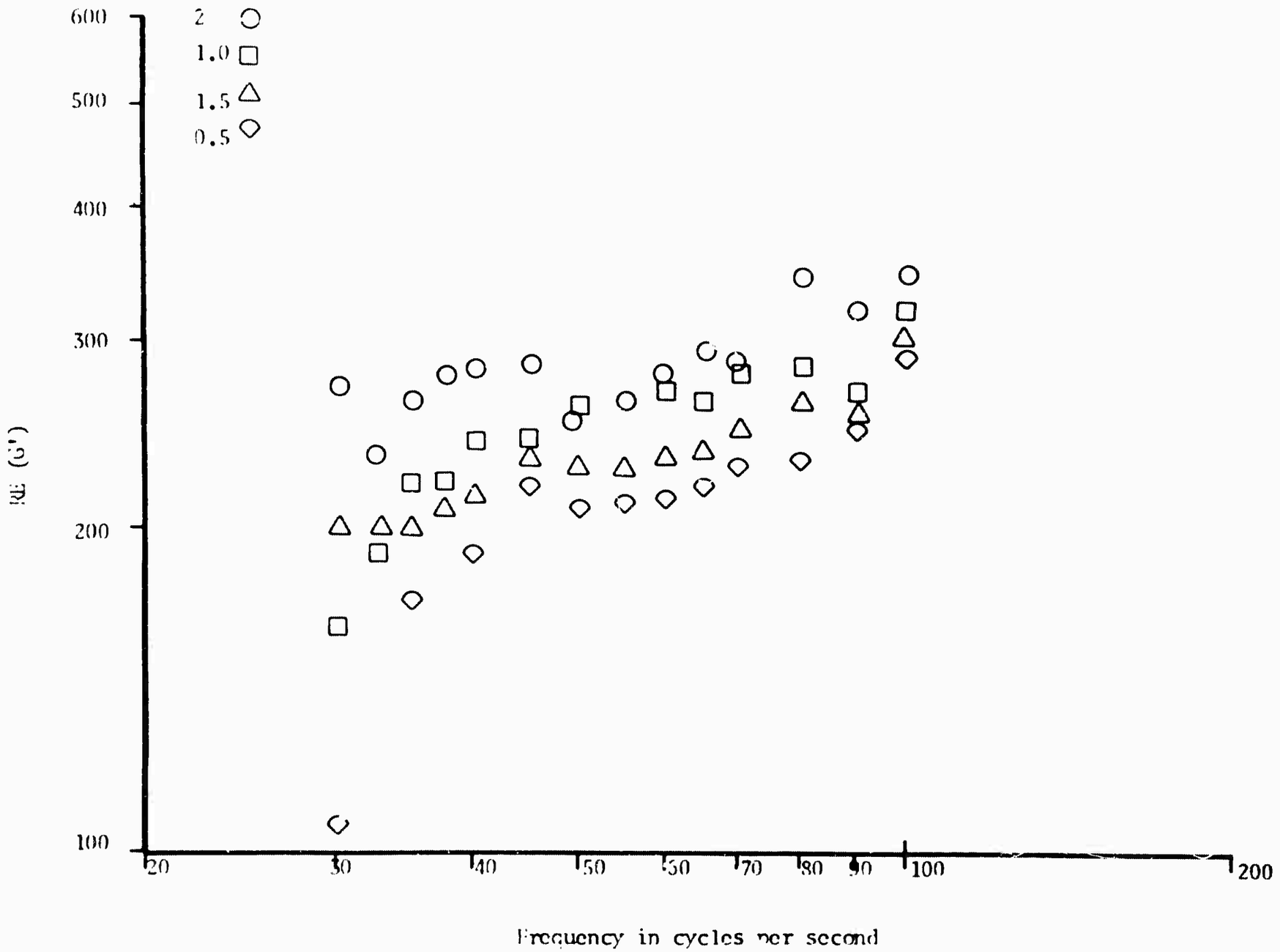

FIG. 6 EFFECT OF LENGTH ON SHEAR MODULUS.

FIG. 7 INFLUENCE OF NOISE ON SIGNAL WHEN MEASURED BY A TRUE R.M.S. CIRCUIT

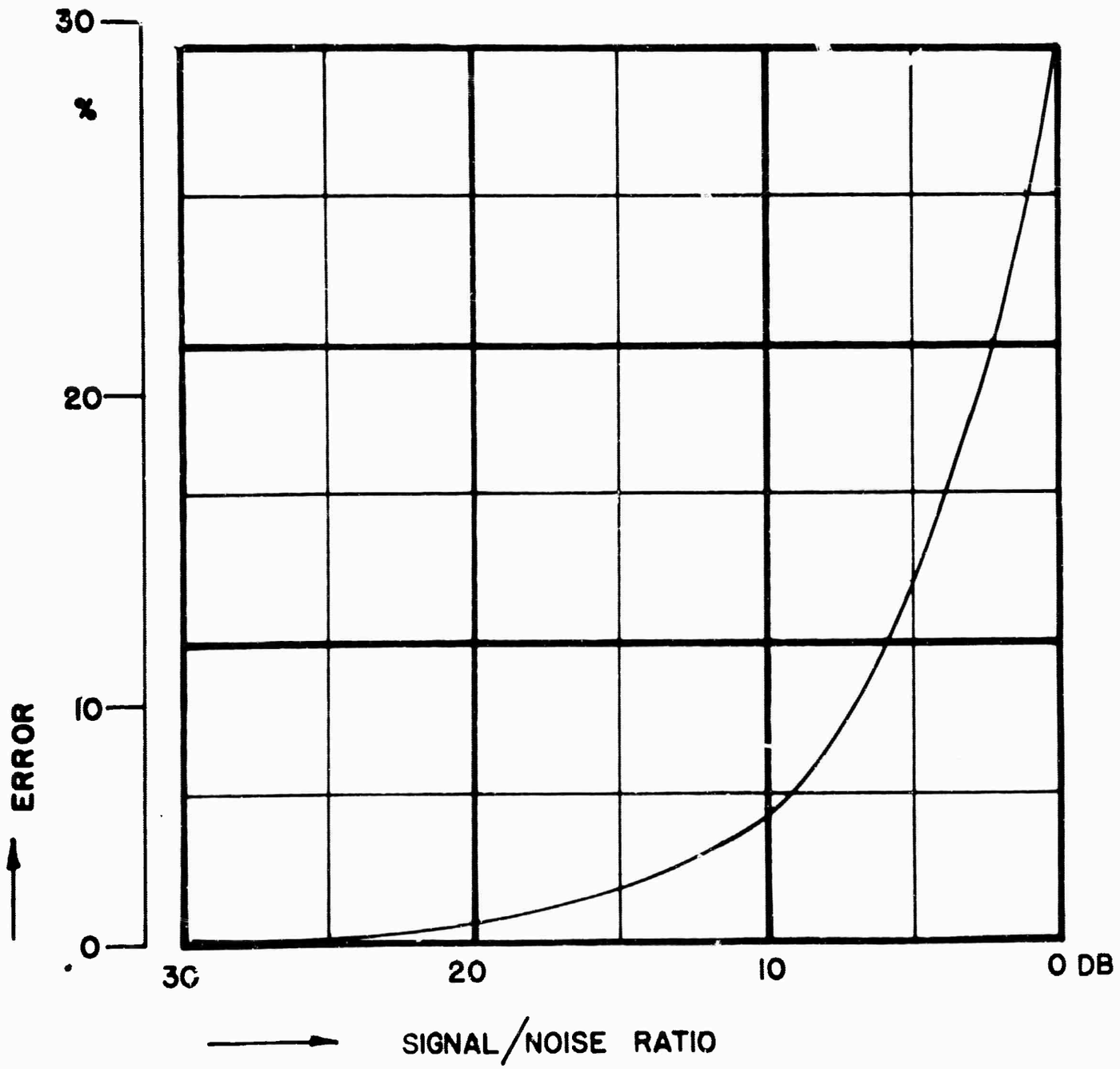

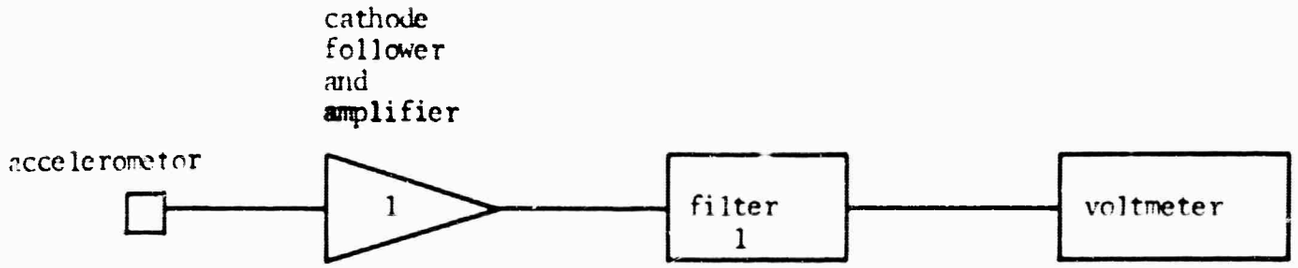

a. Amplitude Measuring Circuit

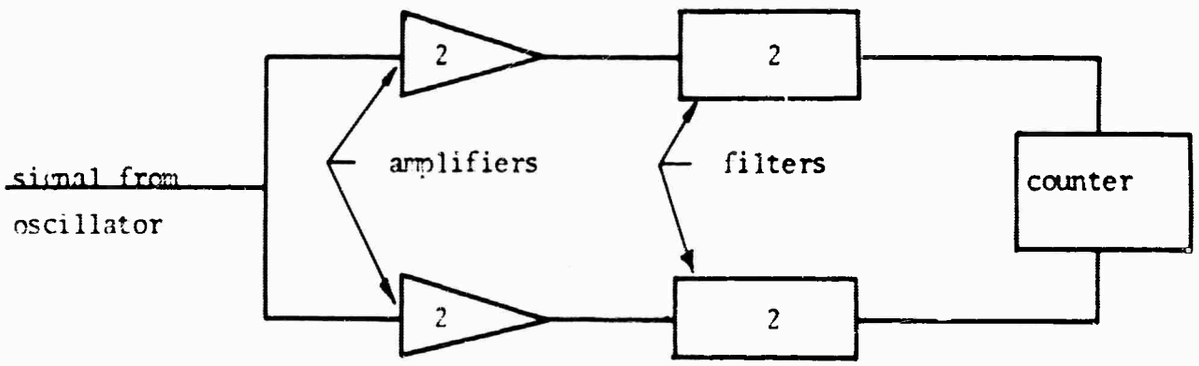

b. Phase Compensating Circuit

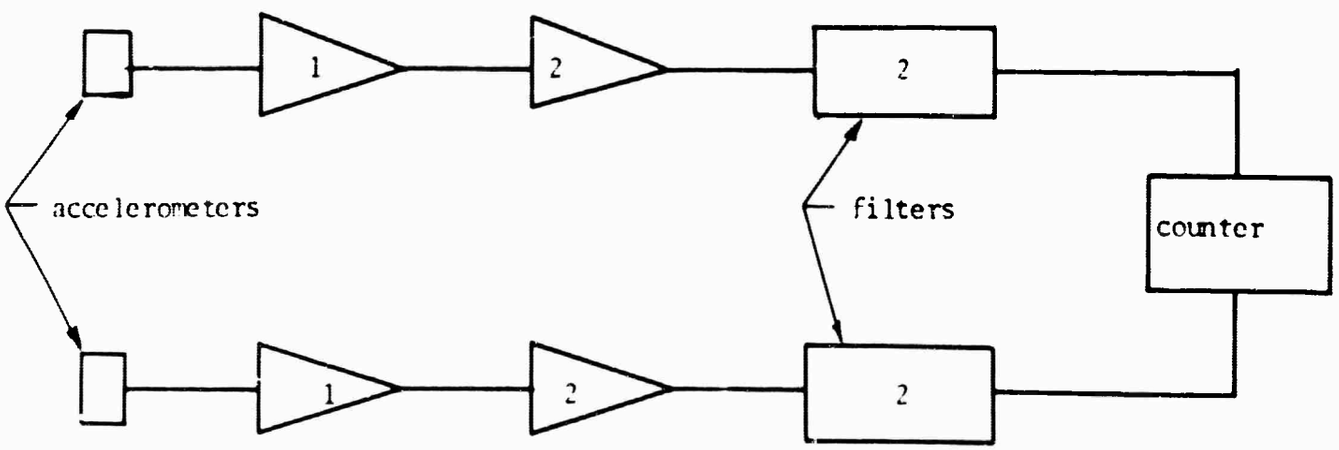

c. Frequency and Phase Measuring Circuit in Operational Mode

FIG. 8 VARIOUS CIRCUITS IN THE DATA ACQUISITION SYSTEM.

DETERMINATION OF THE DYNAMIC YOUNGS MODULUS AND STRESS OPTIC COEFFICIENT OF HYSOL 4485

I. Theory

The theory used in this report was that for the longitudinal vibration of a one-dimensional linearly visco-elastic column excited sinusoidally at one end. There was no deviation from the solution of Brown and Selway (5) for the equation of motion

$$\frac{\partial \sigma}{\partial x} = \rho \frac{\partial^2 u}{\partial t^2} \qquad (1)$$

where σ = the longitudinal stress

x = the longitudinal displacement

ρ = the mass density

u = the particle displacement

t = time

On the assumption that HYSOL 4485 is a linearly visco-elastic material, the stress-strain law for sinusoidally varying stresses is

$$\frac{\sigma}{e} = E^* e^{i\phi} \qquad (2)$$

where E^* = the dynamic elastic modulus

ϕ = the phase angle by which strain lags stress

Now the linear visco-elastic equation of motion is

$$\frac{\partial^2 u}{\partial x^2} = \frac{e^{-i\phi}}{c^2} \frac{\partial^2 u}{\partial t^2} \qquad (3)$$

where $c = \sqrt{\frac{E^*}{\rho}}$

From the solution of equation (3), Brown and Selway obtain

$$\phi = 2 \tan^{-1} \left[\frac{2}{(2m-1)\pi} \sinh^{-1} \left(\frac{U_L}{U_o} \right) \right], \quad m = 1,2,3.... \qquad (4)$$

and

$$c = \frac{2\omega_r L \cos\left(\frac{\phi}{2}\right)}{(2m-1)\pi}, \quad m = 1, 2, 3, ... \qquad (5)$$

where M = mode number

U_L = the driven end displacement amplitude

U_o = the free end displacement amplitude

L = total length of the specimen

ω_r = a resonant frequency corresponding to m = 1, 2, 3, etc.

Equations (4) and (5) were used to calculate ϕ and c from measured values of U_L/U_o at resonance. The dynamic modulus was then calculated from

$$E^* = \rho c^2 \qquad (6)$$

II. Stress Equation

The displacement expression (solution of equation (3)) was differentiated with respect to x to obtain the strain expression. The strain expression was substituted into the stress-

strain law, Eq. (2), to obtain the stress expression

$$\sigma(x,t) = -\frac{U_L}{\beta_L}\rho\omega c\left[\gamma(x)\right]^2 + \left[\delta(x)\right]^2 e^{\left[\omega t + \frac{\phi}{2} - \tan^{-1}\frac{\gamma(x)}{\delta(x)}\right]} \quad (7)$$

At resonance, we only deal with the amplitude of this expression and then

$$\left|\beta_L\right| = \left|\frac{U_L}{U_o}\right| \quad (8)$$

and

$$\gamma(x) = \sin\left(\frac{\omega x}{c}\cos\frac{\phi}{2}\right)\cosh\left(\frac{\omega x}{c}\sin\frac{\phi}{2}\right)$$

$$\delta(x) = \cos\left(\frac{\omega x}{c}\cos\frac{\phi}{2}\right)\sinh\left(\frac{\omega x}{c}\sin\frac{\phi}{2}\right) \quad (9)$$

III. Optical Frequency Response

The dynamic stress optic coefficient, F*, was determined by taking the ratio of the stress amplitude at the driven end to the maximum fringe value at the driven end at resonance, or

$$F^* = -\frac{U_L \rho\omega c}{\delta L m_{max}}\sqrt{\left[\gamma(L)\right]^2 + \left[\delta(L)\right]^2} \quad (10)$$

IV. Apparatus and Procedure

Test Specimen

The HYSOL 4485 specimen used was of dimensions 1/2" x 3/4" x 10", longer and thicker than the one used by Brown and Selway (6). Twenty-two stations were established with an opaque black ink coating on all of the odd-numbered space and covering

half of the specimen width. A 1/2 x 3/4 x 3/4 epoxy head was bonded to the upper end of the specimen with Eastman 910 cement. An iron-constantan thermocouple was included in a slight central depression of the interface for monitoring the specimen temperature.

Birefringence and Displacement Recording Equipment

The physical arrangement of the equipment was identical with that used by Brown and Selway (6) with four exceptions: (a) the light source was replaced by a Spectra Physics Model 130 continuous wave 6328A laser; (b) quarter wave plates adjusted to 6328A were used; (c) a kronhite filter, model 350-A, was inserted between the photomultiplier tube and the oscilloscope to eliminate troublesome noise, and; (e) no additional optical components were used. It is interesting to note that the red laser beam resulted in an output of the EMI 95365 photomultiplier tube two orders of magnitude greater than that obtained with the previous green light source. Since only one laser was available and because it was impractical to split the 3 millimeter beam into two parts, two series of tests were run; one for the displacement data and one for the birefringence data.

The Tardy method of rotating the analyzer to obtain maximum or minimum light transmission, with the polarizer parallel

to the principal stress direction, was used to evaluate fractional order fringes.

The phase angle β between the displacement at any point and the displacement at the driven end was found by referring the photomultiplier output to the shaker accelerometer, after inverting the sign of the accelerometer signal.

The phase angle, ϕ, between stress and strain was calculated from the experimental values of U_L/U_o.

The static value of the stress optic coefficient, F, was determined by applying incremental weights of 0.1 pound, or 0.267 p.s.i., and noting the fractional fringe order using the laser and a vacuum tube voltmeter. The time elapsed was one minute per load increment. Strain was noted on an N-type SR-4 strain indicator as measured by two very flexible clip gages. These U-shaped clip gages were hard phosphor bronze and measured 0.020" thick x 0.30" wide x 2.0" long and stood 1-1/2" from each side of the HYSOL 4485 specimen. The ends of the clip gages were bonded to the 1/2" x 3/4" x 6" specimen with Eastman 910 cement by means of a 0.020" x 3/16" x 3/4" foot. Negligible force was carried by the clip gage in comparison to that supported by the specimen. A tension and compression foil resistance strain gage on each side of the "pure bending" section of each clip gage constituted the four legs of a Wheatstone bridge.

V. Results and Discussion

The mechanical behavior of HYSOL 4485 was found to be quite sensitive to a change in temperature. The thermocouple in the interface between the polyurethane specimen and the epoxy holder indicated a range of temperatures from 79°F to 84°F during the recording of the displacement data. Consistent, smooth displacement curves were obtained. An interface temperature variation from 86°F to 103°F was recorded during the recording of photoelastic data. Since room temperature did not exceed 90°F, the high specimen temperature recorded during the fourth and fifth mode vibration was probably a result of using a higher input power level in order to delineate the low order fringes. The jump in fringe constant between the third and fourth mode (figure 17) may be attributable to the jump in temperature.

Resonant Frequencies

A determination was made of the experimental phase angle between driven end and free end displacements (ϕ_L) as a function of frequency. The "resonant" frequencies at which this angle was 90°, 270°, 450°, 630°, and 810° constituted the first five resonant modes and they occurred at 41, 199, 345, 500 and 638 cycles per second.

Experimental and Theoretical Displacement Data

Figures 10 and 13 show the experimental (points) and theoretical (curves) displacement amplitudes and phase angles for

the second to the fifth resonant frequencies. A very close proximity between the fundamental longitudinal mode and one of the higher bending modes made it impossible to obtain stable displacement data at 41 cycles per second. Agreement is generally good for the other modes. Discrepancies or lack of data at some locations on the specimen were caused by coupling between the sometimes present bending mode and the longitudinal mode. Wave theory indicates that as the frequency increases, and the wave length decreases, the one-dimensional theory used here will break down. However, at frequencies up to 638 cycles per second, this effect was not observed. It would therefore seem that the one-dimensional theory is adequate for the current response of HYSOL 4485 of dimensions 1/2 x 3/4 x 10" in the frequency range up to 638 cycles per second.

Experimental Isochromatic Data

The experimental stress fringes are shown in figures 14 to 16 as a function of X/L for the five resonant modes. An upper and lower set of data are shown; the upper set corresponds to rotating the analyzer clockwise and the lower set counterclockwise. The average of the two sets was taken as the true datum. No theoretical fringes were predicted since this calculation would only verify, by a correspondence between the theoretical and experimental fringes, that we were dealing with a linear visco-

elastic material. Instead, the power input was reduced to 0.53 of the usual value for the second mode case and the fringe orders were reduced to 0.49 $\pm$ 4% of their original values. In this way HYSOL 4485 was demonstrated to be an approximately linear visco-elastic material at 200 cycles per second.

Since HYSOL 4485 is a linear visco-elastic material, its mechanical and optical properties are characterized by the frequency dependence of the dynamic modulus, E*, the stress-strain phase angle, o, and the dynamic stress-optic coefficient, F*. These results are presented in figure 17. The strain optic coefficient is not included since strain was not measured directly and could only be inferred from the displacement data. The stress-fringe phase angle, determinations were so inaccurate as to be inconclusive and are not presented here.

Conclusions

The 1/2 x 3/4 x 10" HYSOL column, when resonating in any one of the first five longitudinal modes, followed the linear one dimensional visco-elastic theory. The frequency range was 0 to 650 cps and the highest stress amplitude was 24 psi; a value 1-1/2 times as high as that used by Brown and Selway.

At an average temperature of 82°F. modulus, E*, varied from 680 psi at 200 cps to 800 psi at 650 cps, with a static value, E, of exactly 400 psi. At an average temperature of 94° F. the

stress-optic coefficient, F*, varied from 1.0 to 2.8 psi/finge/ inch. The stress-strain phase angle increased from 9.8° at 200 cps to 12.4° at 650 cps.

The very inaccurate stress-fringe phase angles were not included. However, birefringence did lag both stress and strain.

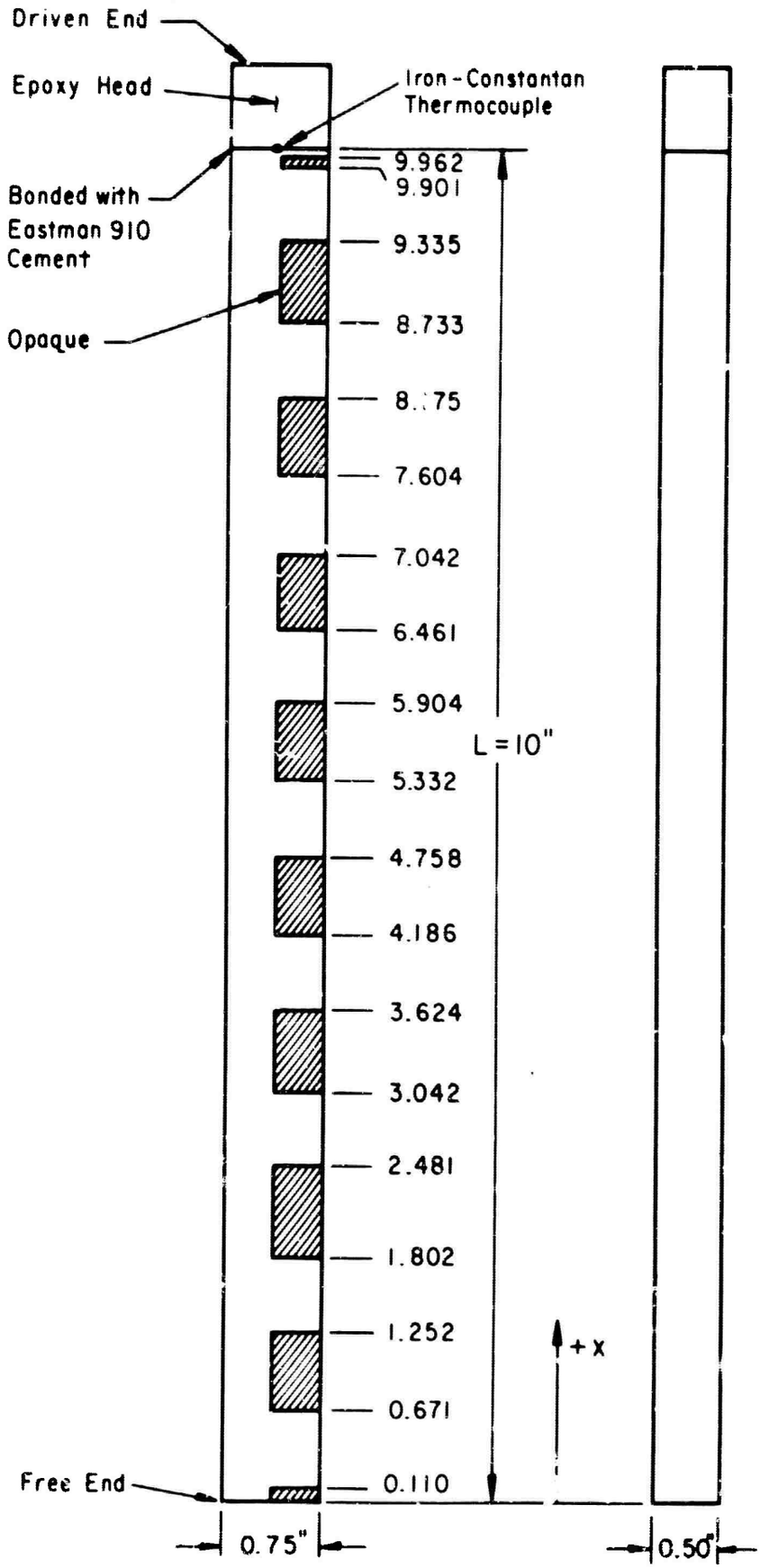

FIG. 9. TEST SPECIMEN.

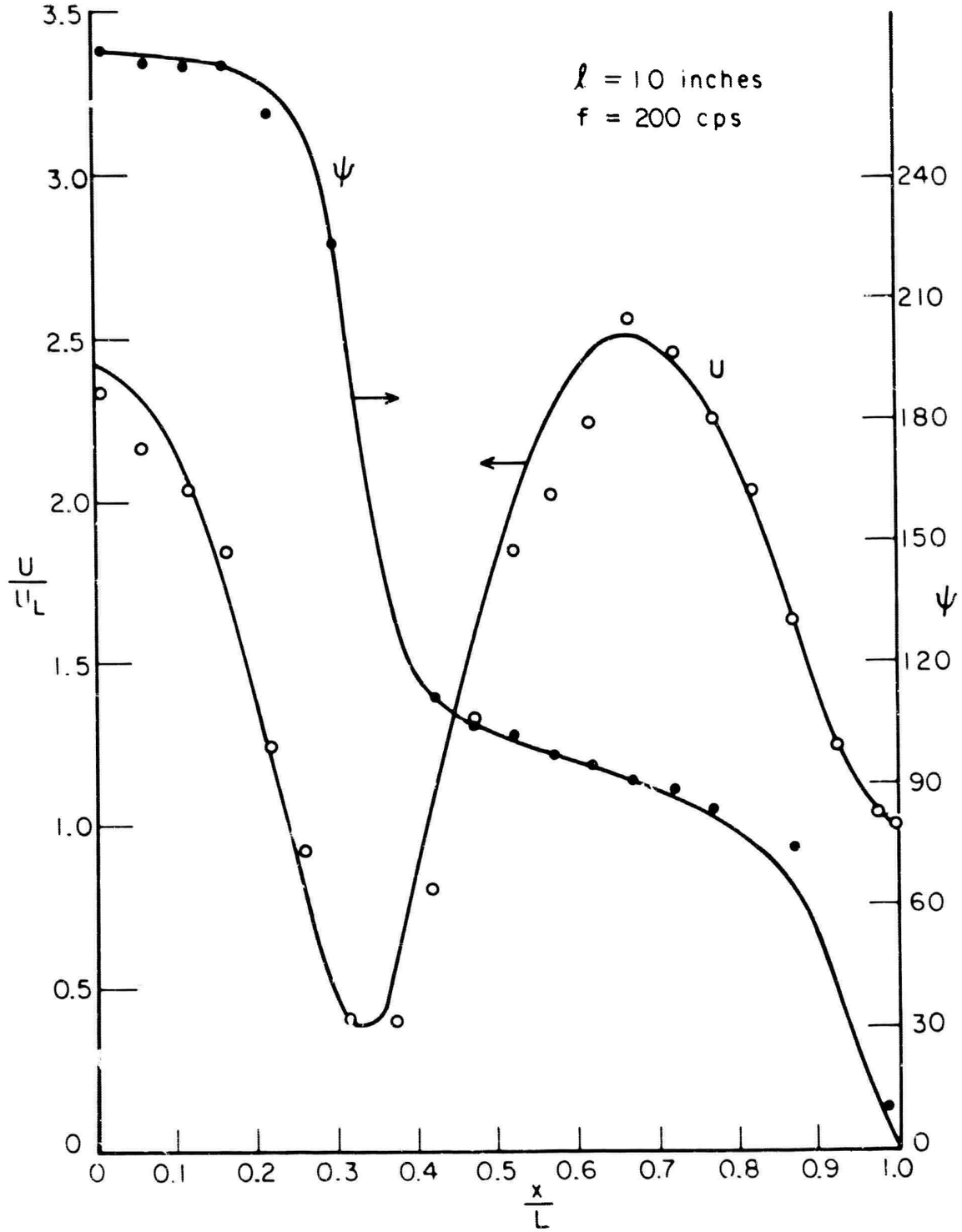

FIG. 10. THEORETICAL AND EXPERIMENTAL DISPLACEMENT AND PHASE ANGLES FOR THE SECOND RESONANT FREQUENCY.

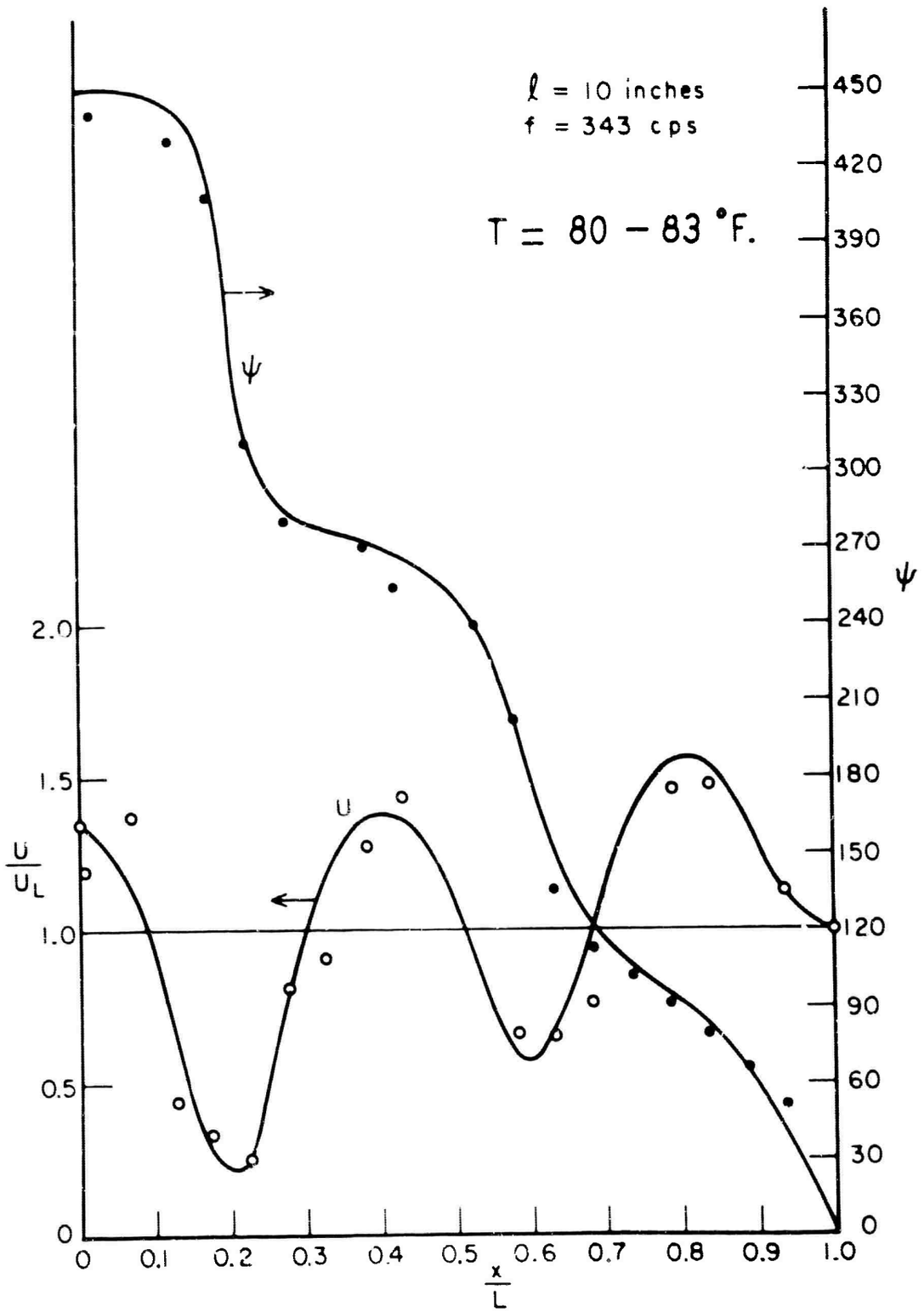

FIG. 11. THEORETICAL AND EXPERIMENTAL DISPLACEMENT AND PHASE ANGLES FOR THE THIRD RESONANT FREQUENCY.

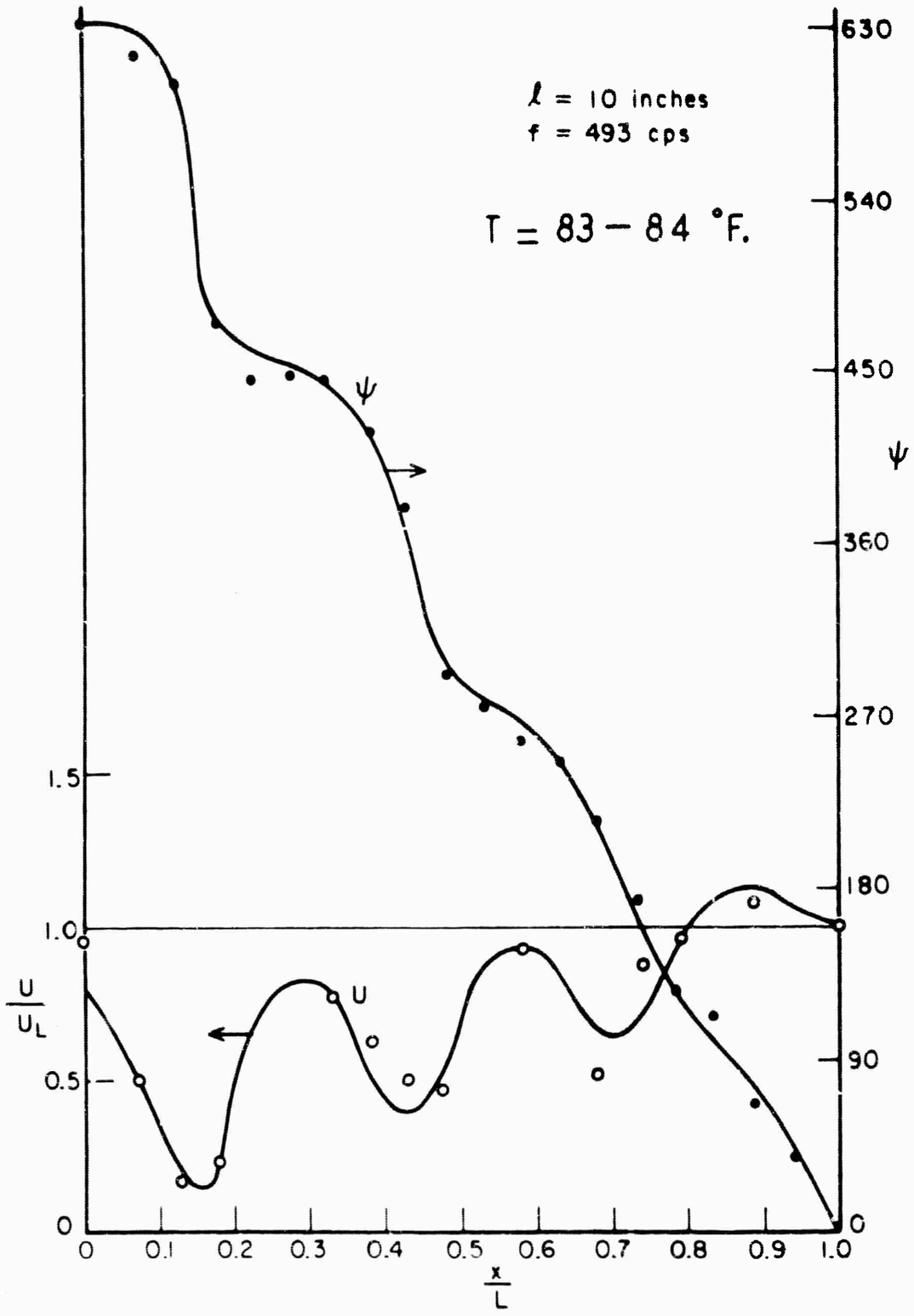

FIG. 12. THEORETICAL AND EXPERIMENTAL DISPLACEMENT AND PHASE ANGLES FOR THE FOURTH RESONANT FREQUENCY.

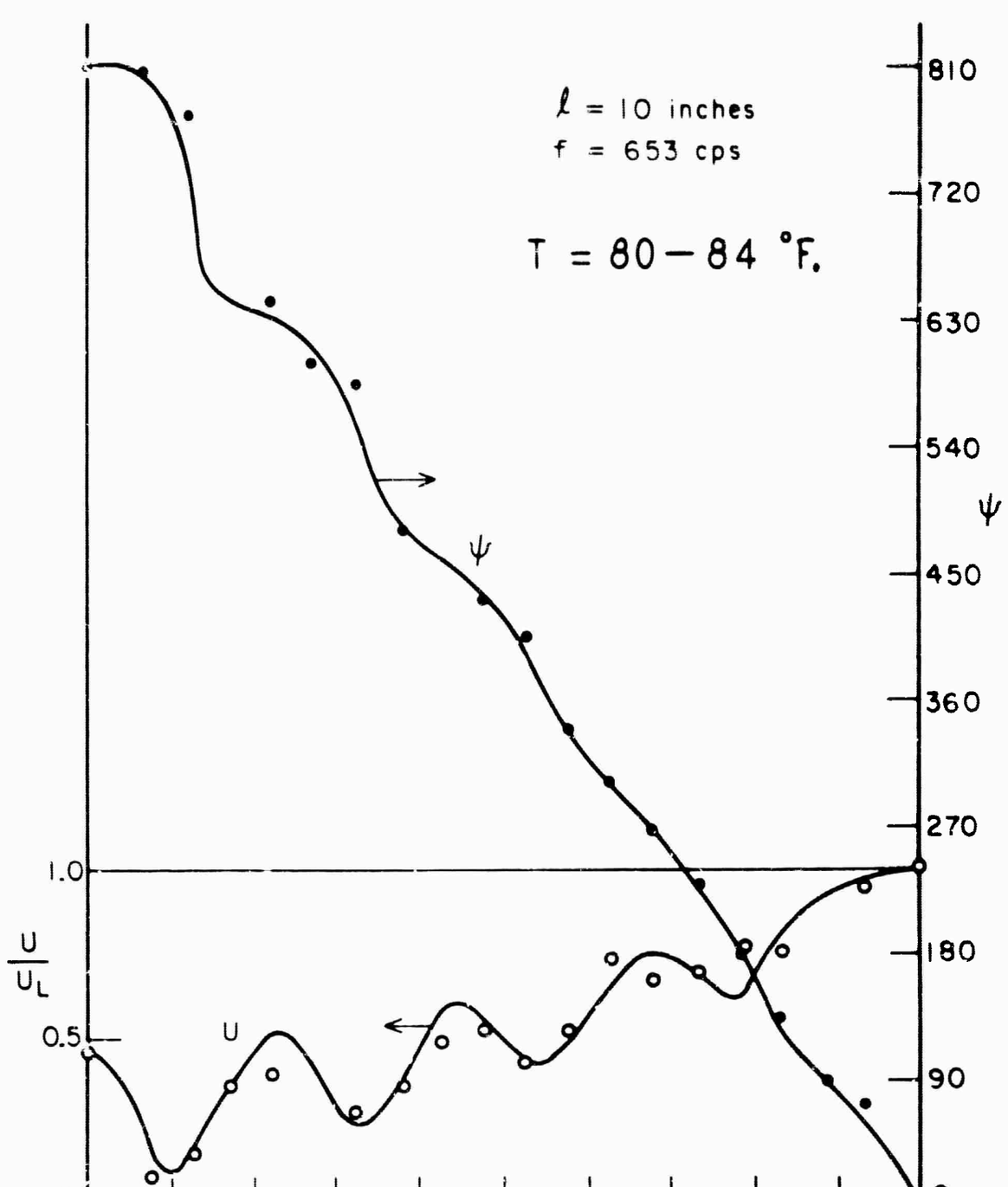

FIG. 13. THEORETICAL AND EXPERIMENTAL DISPLACEMENT AND PHASE ANGLES FOR THE FIFTH RESONANT FREQUENCY.

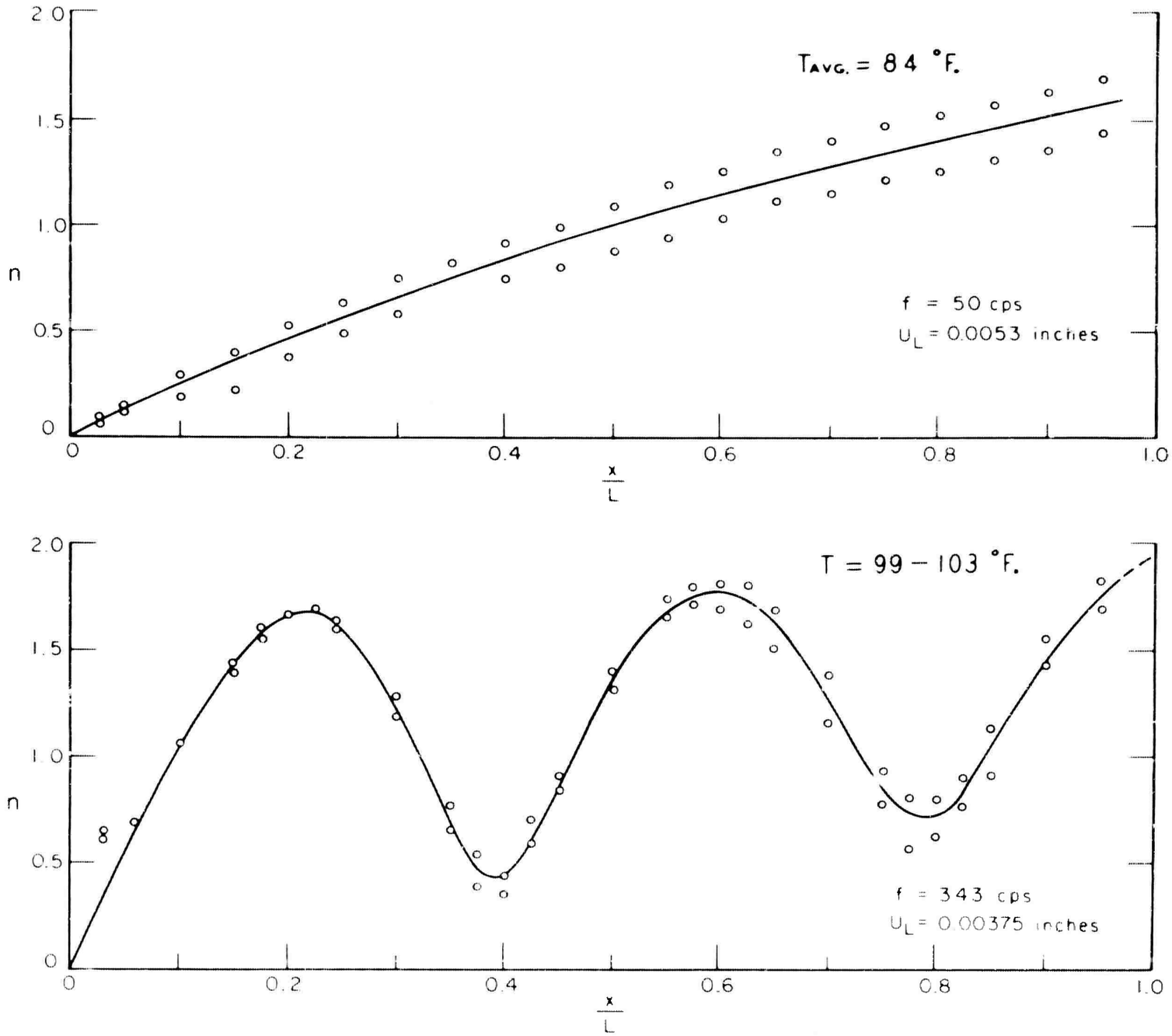

FIG. 14. EXPERIMENTAL FRINGE ORDERS FOR THE FIRST AND THIRD RESONANT FREQUENCIES.

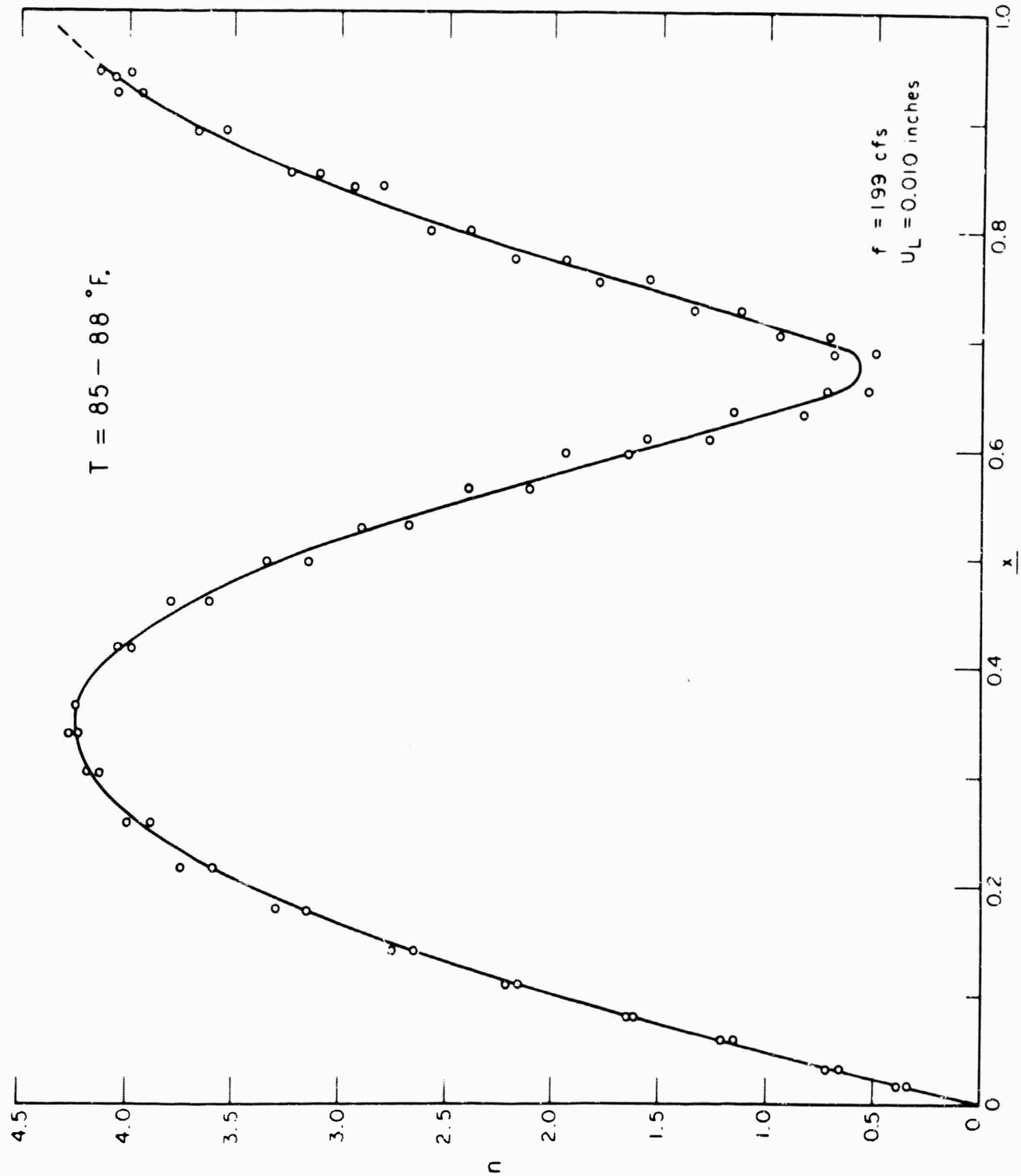

FIG. 15. EXPERIMENTAL FRINGE ORDERS FOR THE SECOND RESONANT FREQUENCY.

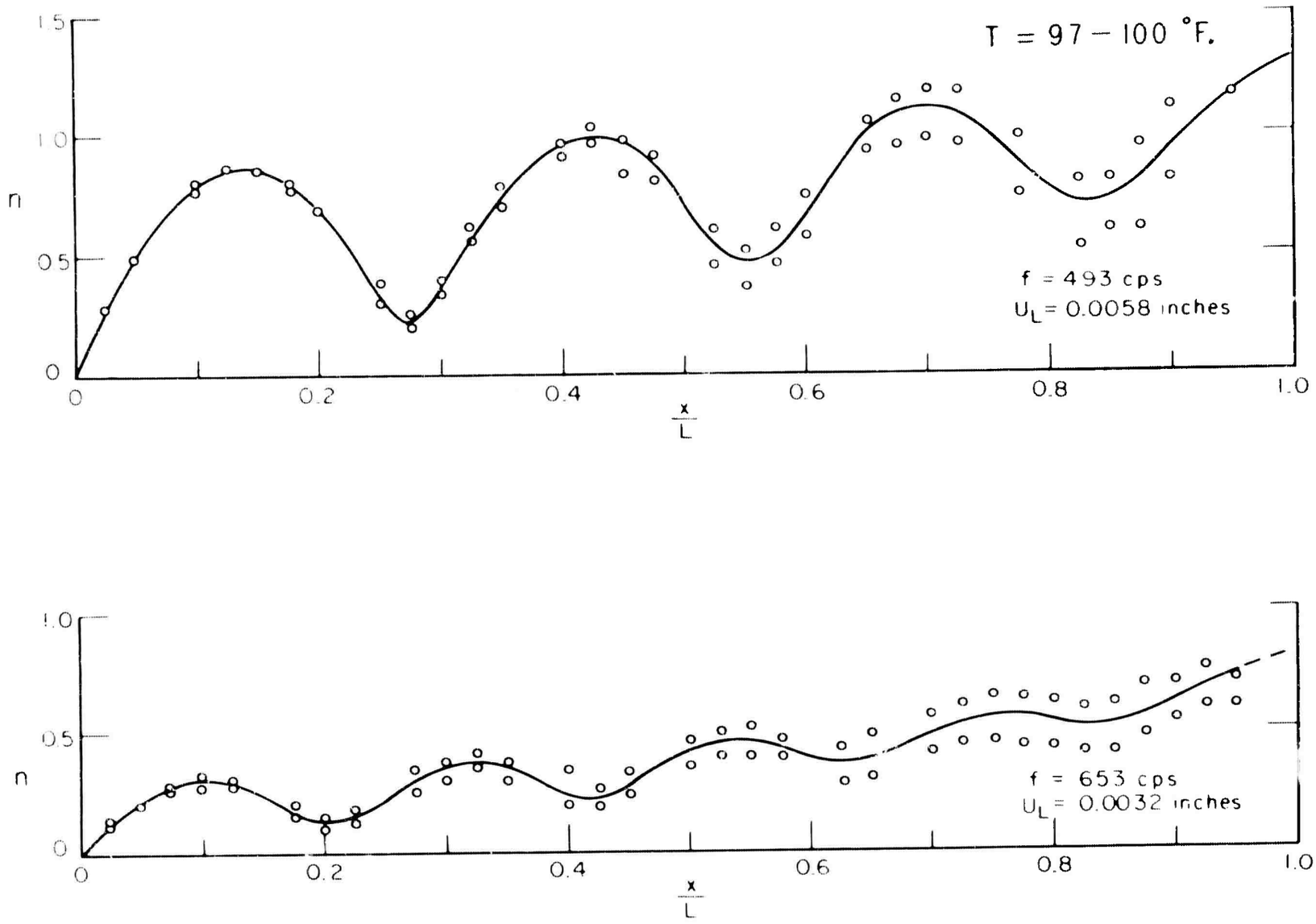

FIG. 16. EXPERIMENTAL FRINGE ORDERS FOR THE FOURTH AND FIFTH RESONANT FREQUENCIES.

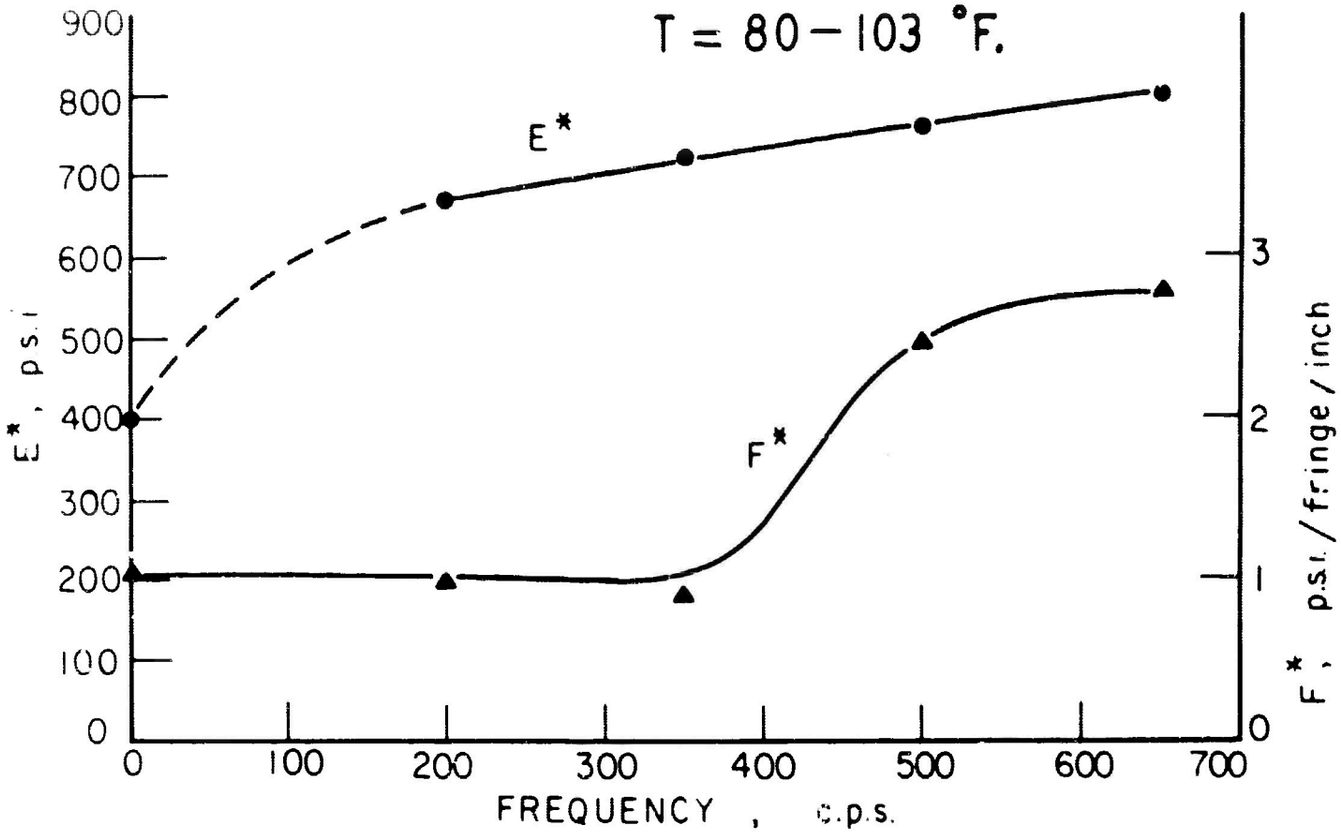

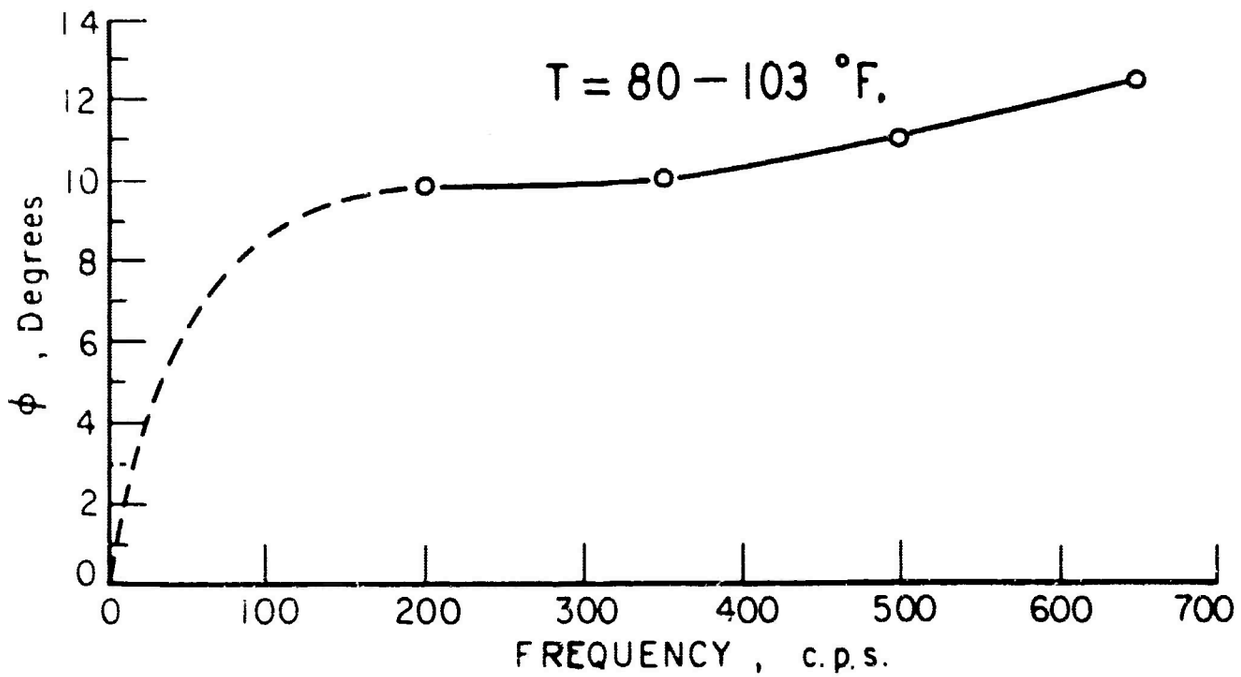

FIG. 17. MECHANICAL AND OPTICAL FREQUENCY RESPONSE OF HYSOL 4485 FROM 0 TO 650 C.P.S.

DETERMINATION OF THE STATIC AND DYNAMIC PROPERTIES OF HYSOL 4485

1. INTRODUCTION

The research program covered by this report was conducted to determine the static and dynamic mechanical and optical properties of a pour of HYSOL 4485 used in the fabrication of a group of rectangular plates. The plates were cast by Hysol Corporation for Boston College under Armour Research Foundation Purchase Order No. 46949. All of the specimens used for the determinations were cut from material which remained after 12" x 12" test plates were removed from the larger plates provided by the supplier.

The static properties which were determined include:

a) Photoelastic stress fringe value

b) Modulus of elasticity

c) Poisson's ratio

The dynamic properties which were determined include:

a) Modulus of elasticity

b) Shear modulus

c) Photoelastic stress fringe value

The modulus of elasticity and shear modulus were determined for a limited range of frequencies between 100 and 600 cycles per

second. Funds available for the program were not sufficient to permit similar determinations to be made of the photoelastic stress fringe value.

II. STATIC PROPERTIES

A. Photoelastic Stress Fringe Value

The static photoelastic material fringe value was obtained by subjecting a 3 inch diameter disk of the material to increments of diametral load and recording the fringe order at the center of the disk for each increment with a 12 inch diameter diffused light polariscope. The Tardy method of compensation was used to establish the fractional fringe orders. The maximum shear stress at the center of the disk as presented in a well known analytical solution is as follows:

$$\tau_{max} = \frac{\sigma_1 - \sigma_2}{2} = \frac{4P}{\pi t D}$$

where τ_{max} = maximum shear stress

σ_1, σ_2 = principal stress

P = diametral load

D = diameter of disk

t = thickness of disk

From the static stress-optic law

$$\tau_{max} = \frac{nf}{t}$$

where n = fringe order at center of disk

f = material stress fringe value in shear

Figure 18 shows the curve obtained by plotting $t\tau_{max.}$ vs. fringe order. The slope of this curve was taken as the material fringe value and was found to be 0.486 psi/fringe/in.

B. Modulus of Elasticity and Poisson's Ratio

The modulus of elasticity and Poisson's ratio (as a function of time under load) were obtained from creep data by utilizing the Moire method of analysis. Two specimens were used for the study. One, which was subjected to a stress level of approximately 20 psi, had two 1000 line per inch arrays printed in the axial and transverse directions. An identical master grid was placed in contact with the model grid and fixed to the loading fixture. A constant load was applied to the specimen and the change in the fringe spacing produced by interference between the two sets of lines were recorded at different times by taking photographs of the specimen. At any time t the longitudinal and transverse strains were computed using

$$\epsilon_i^e = \frac{\Delta n_i}{\Delta x_i} \frac{1}{N}$$

where

$\frac{\Delta n_i}{\Delta x_i}$ = number of fringes/in

N = line spacing of Moire pattern

ϵ_i^e = Eulerian strain

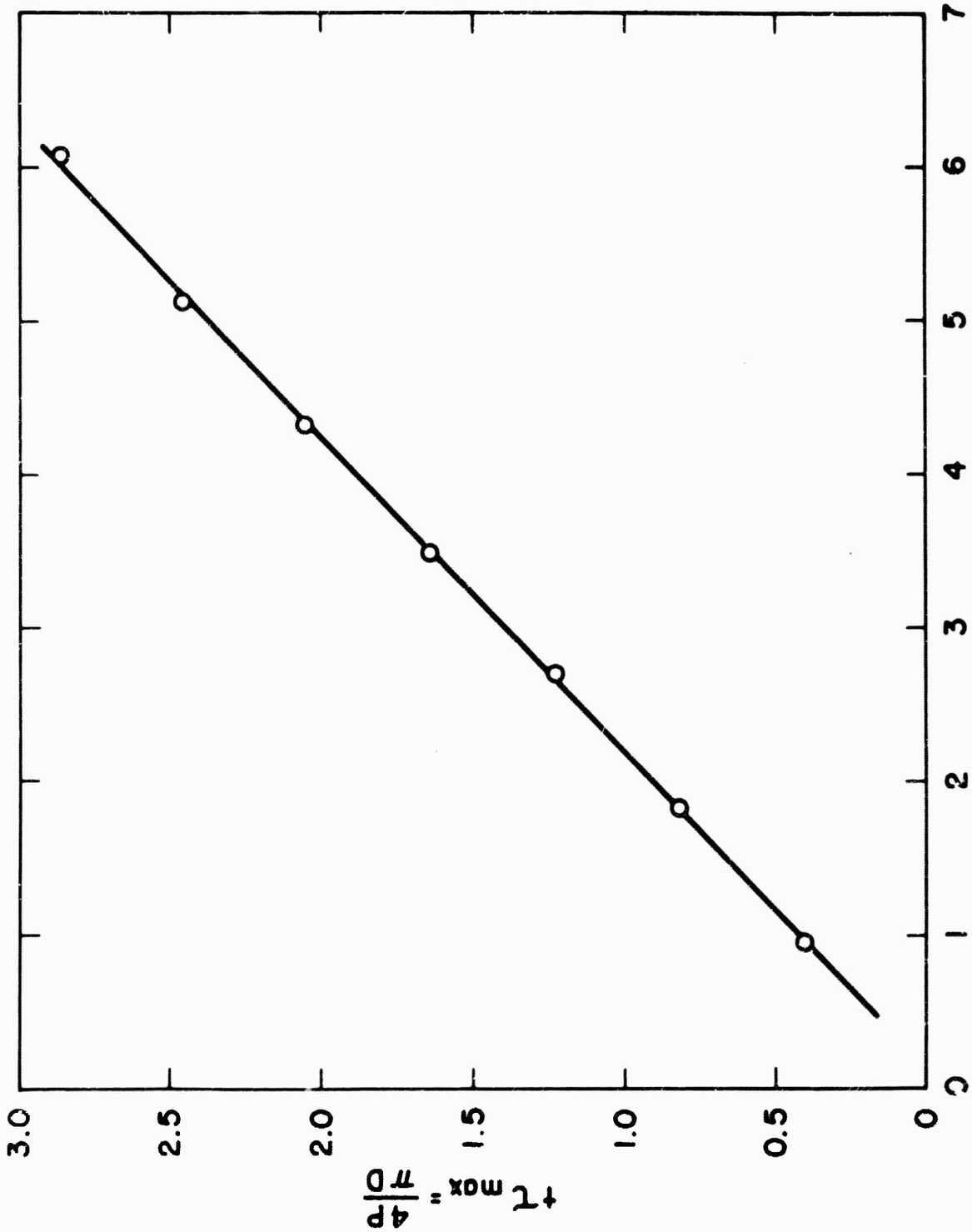

FIG. 18 PLOT OF $t\tau_{max}$ VERSUS FRINGE ORDER n FOR A DISK OF HYSOL 4485 SUBJECTED TO A DIAMETRAL LOAD

To obtain Lagrangian strain, i.e., in terms of the original gage length

$$\epsilon^e = \frac{\ell - \ell_o}{\ell} = 1 - \frac{\ell_o}{\ell}$$

$$\epsilon^L = \frac{\ell - \ell_o}{\ell_o} = \frac{\ell}{\ell_o} - 1$$

$$\epsilon^L = \frac{\epsilon^e}{1 - \epsilon^e}$$

In determining Young's Modulus, the stress was corrected for the decrease in cross sectional area. A plot of the Lagrangian strains and resulting Modulus of Elasticity and Poisson's ratio is given in Fig. 19. Figure 20 shows the results of a creep test at approximately 40 psi stress utilizing 300 line/inch Moire grids on a separate model.

The results of these tests show that the material displays slight viscoelastic properties, but for most practical purposes, it can be considered elastic.

III. Dynamic Properties

The dynamic properties of the HYSOL 4485 material were determined by using both Volterra pendulum (10) and sinusoidal response tests.

A. Volterra Pendulum Studies

The dynamic properties are determined in this method by subjecting a small specimen to the dynamic compression induced

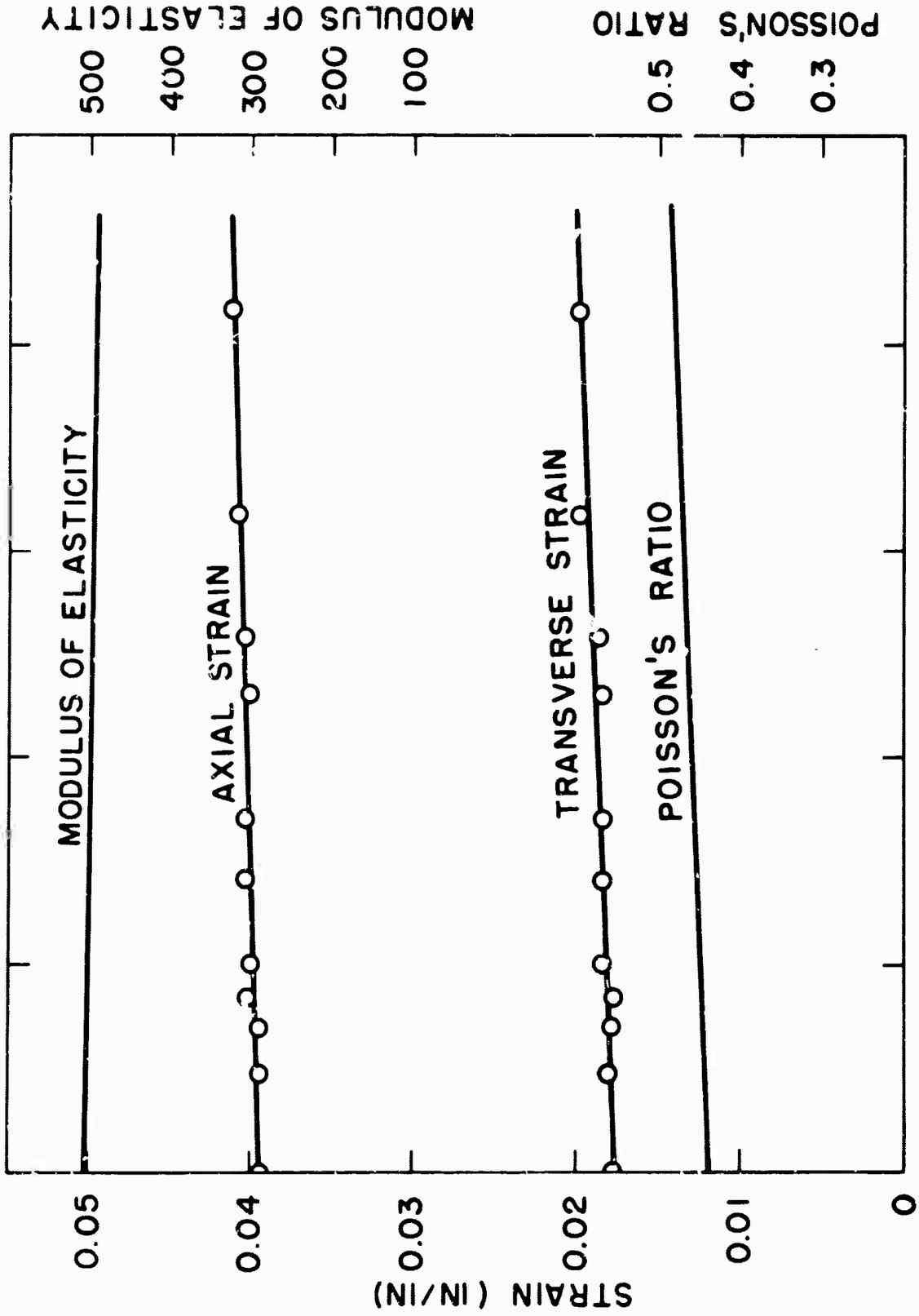

FIG. 19 CURVES SHOWING THE CREEP OF HYSOL 4485 AT A STRESS LEVEL OF 19.96 PSI

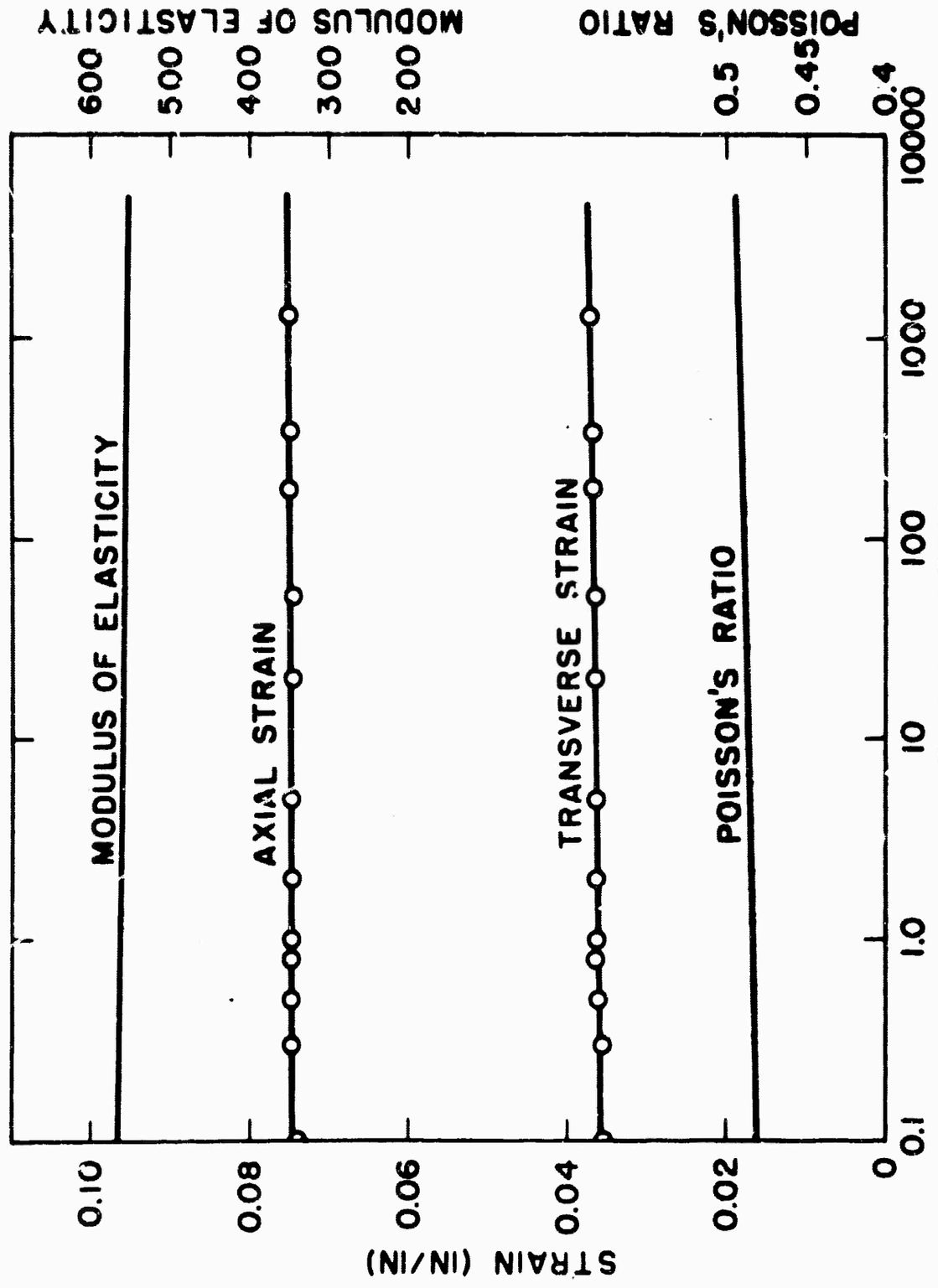

FIG. 20 CURVES SHOWING THE CREEP OF HYSOL 4485 AT A STRESS LEVEL OF 41.58 PSI

by the impact of two metal bars suspended as ballistic pendulums. An accelerometer is mounted on each pendulum to provide a record of the accelerations during impact. The test consists of releasing one pendulum from a desired height and having it strike the specimen which is positioned on the second pendulum. The second pendulum is initially motionless in its equilibrium position. The acceleration traces during impact are recorded by photographing the traces of the accelerometer output voltages on a dual beam oscilloscope. The curves provide sufficient data for the determination of a dynamic stress-strain curve. Curves for the two load levels (20 and 200 psi) investigated in this study are shown in Figs. 21 and 22 respectively.

The dynamic photoelastic properties were obtained by taking high speed photographs of the fringe pattern during impact. The change in fringe order as a function of time over the initial period of impact was correlated to the stress in the specimen over this same time interval to obtain the dynamic material fringe values in terms of stress.

The speed of the camera which was used in the study was determined from timing light traces along the edge of the film to be approximately 17,000 frames per second.

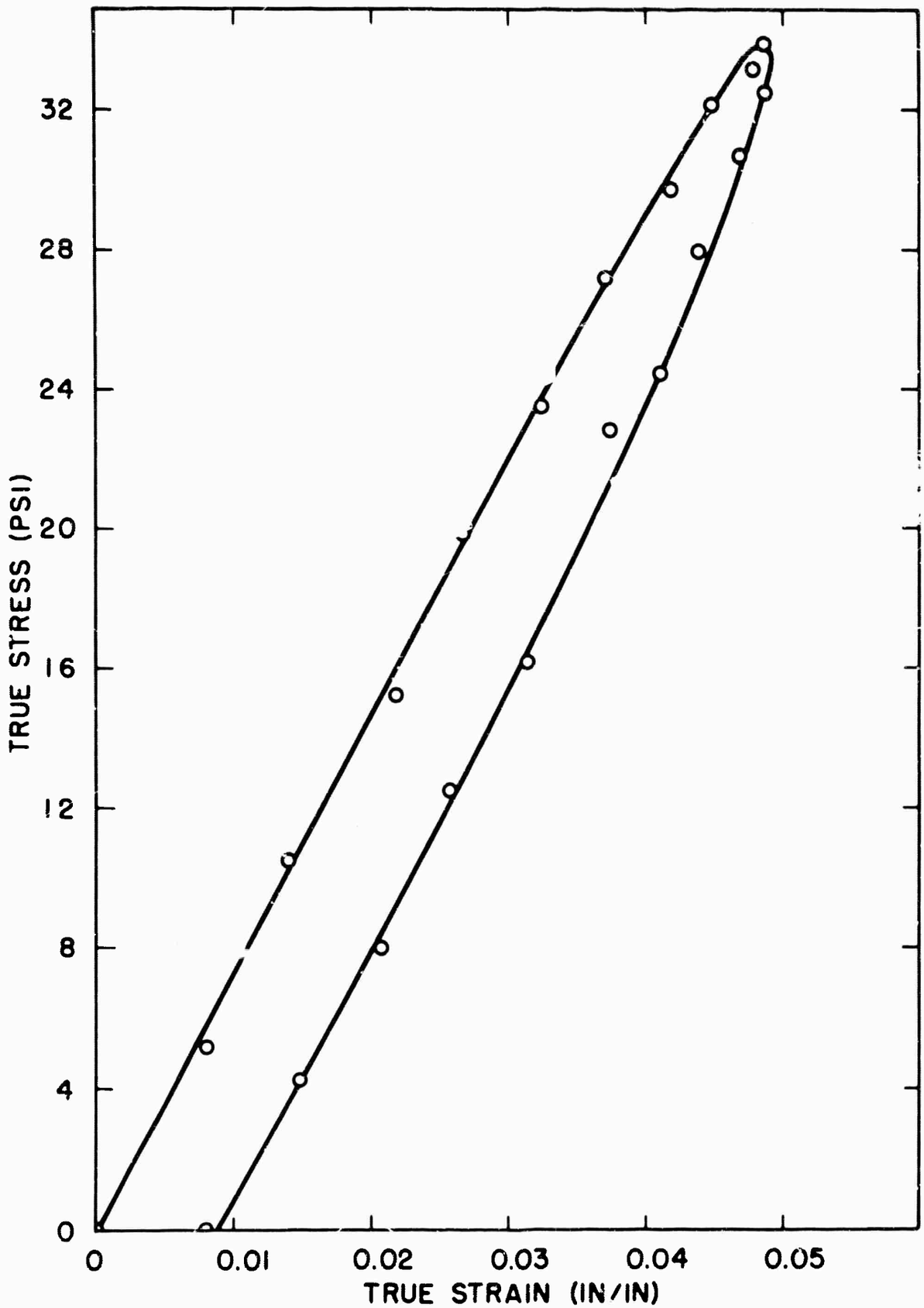

FIG. 21 DYNAMIC STRESS-STRAIN CURVE FOR HYSOL 4485 AT A LOADING RATE OF 7.02 IN/SEC

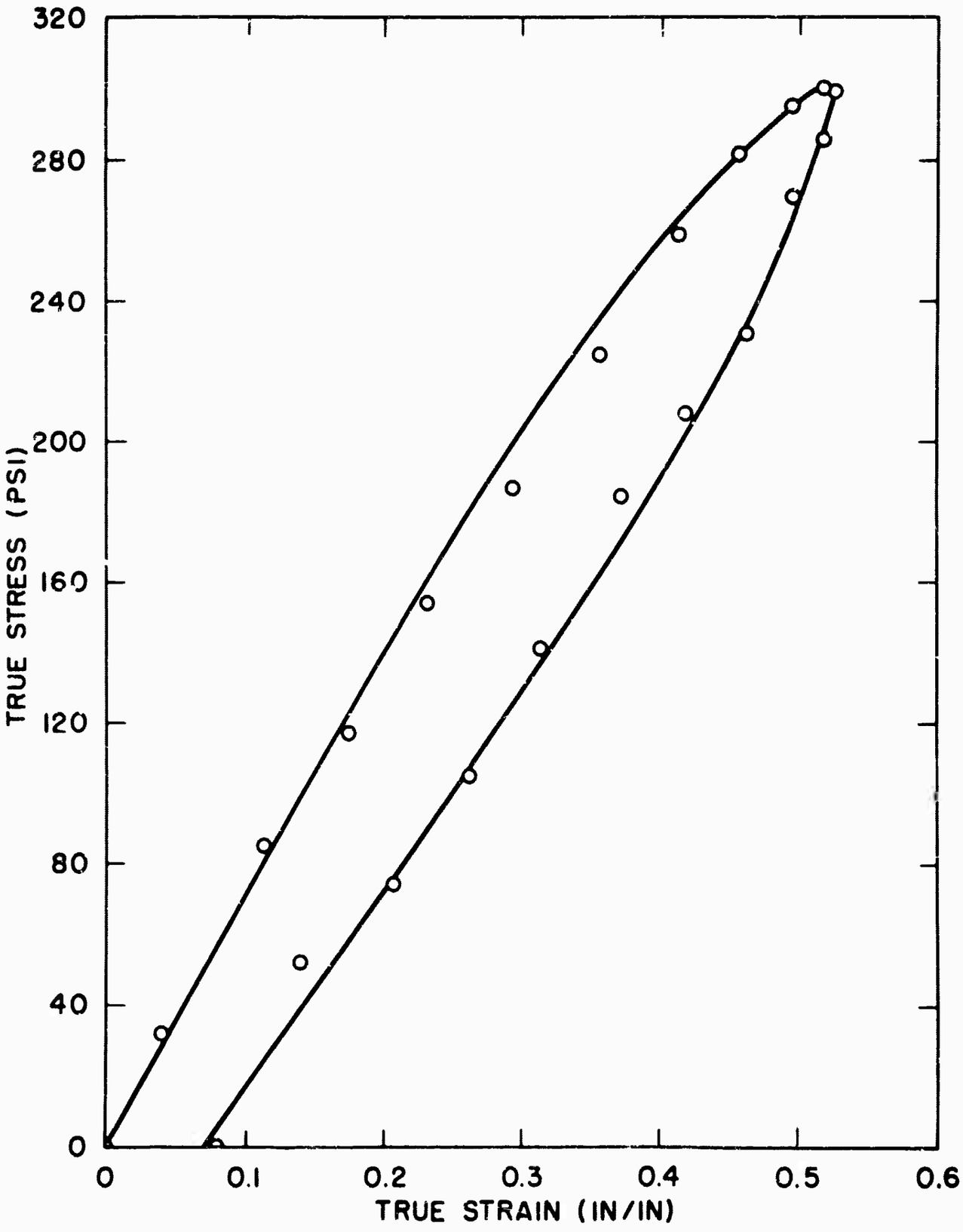

FIG. 22 DYNAMIC STRESS-STRAIN CURVE FOR HYSOL 4485 AT A LOADING RATE OF 65.5 IN/SEC

This speed was sufficient to evaluate the change in fringe order at the low stress level, but at the high stress level, the change in fringe order was too rapid to be evaluated with this camera. Since no faster speeds can be obtained with this camera, no photoelastic data was obtained at the 200 psi level.

From the photographic record of the impact at the 20 psi level a curve of fringe order as a function of time was plotted. This curve which is presented in Fig. 23, shows that the fringe order changes linearly with time over the first millisec of impact. Since the stress over this period of time was also determined to be linear with time, the material fringe value in terms of stress could be determined from the slopes of the stress-time and fringe-time curves. The value obtained was

$$f_\sigma = 0.833 \text{ psi/in-fringe}$$

B. Sinusoidal Response Study

The modulus of elasticity, shear modulus, and phase angle between stress and strain were determined over a limited range of frequencies in this phase of the study. The frequency range could be extended by using specimens of different size but the funds available when the work was conducted was not sufficient to permit this extension of work. The results which were obtained for the frequency range from 100 to 500 cycles

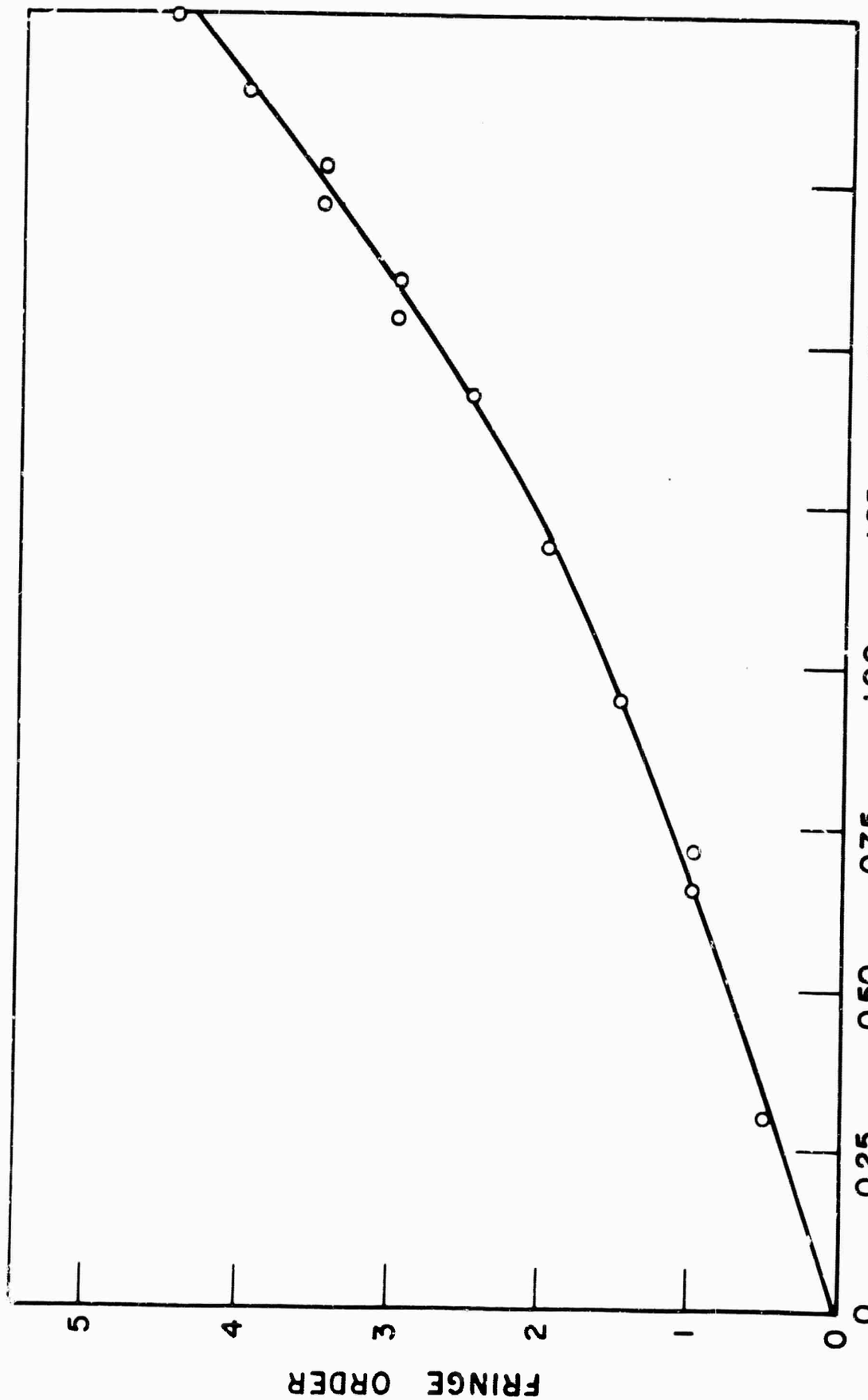

FIG. 23 FRINGE ORDER AS A FUNCTION OF TIME FOR HYSOL 4485 IMPACTED AT A VELOCITY OF 7.02 IN / SEC

per second are shown in Figs. 24 and 25. The absolute values of the moduli are shown together with the phase angles. The real and imaginary components of the complex moduli can be obtained by multiplying by the cosine and sine of the phase angle respectively.

IV. Summary

In the previous sections of this report curves have been presented which show the static and dynamic properties of a material known commercially as HYSOL 4485. In all of the work extreme care has been exercised in order to obtain results whose accuracy represents the best obtainable within the limits of current methods and techniques. As a result we feel that the values presented should vary from the true values by no more than $\pm$ 5 percent. A tabulation of values used in plotting the curves are presented in the tables which follow:

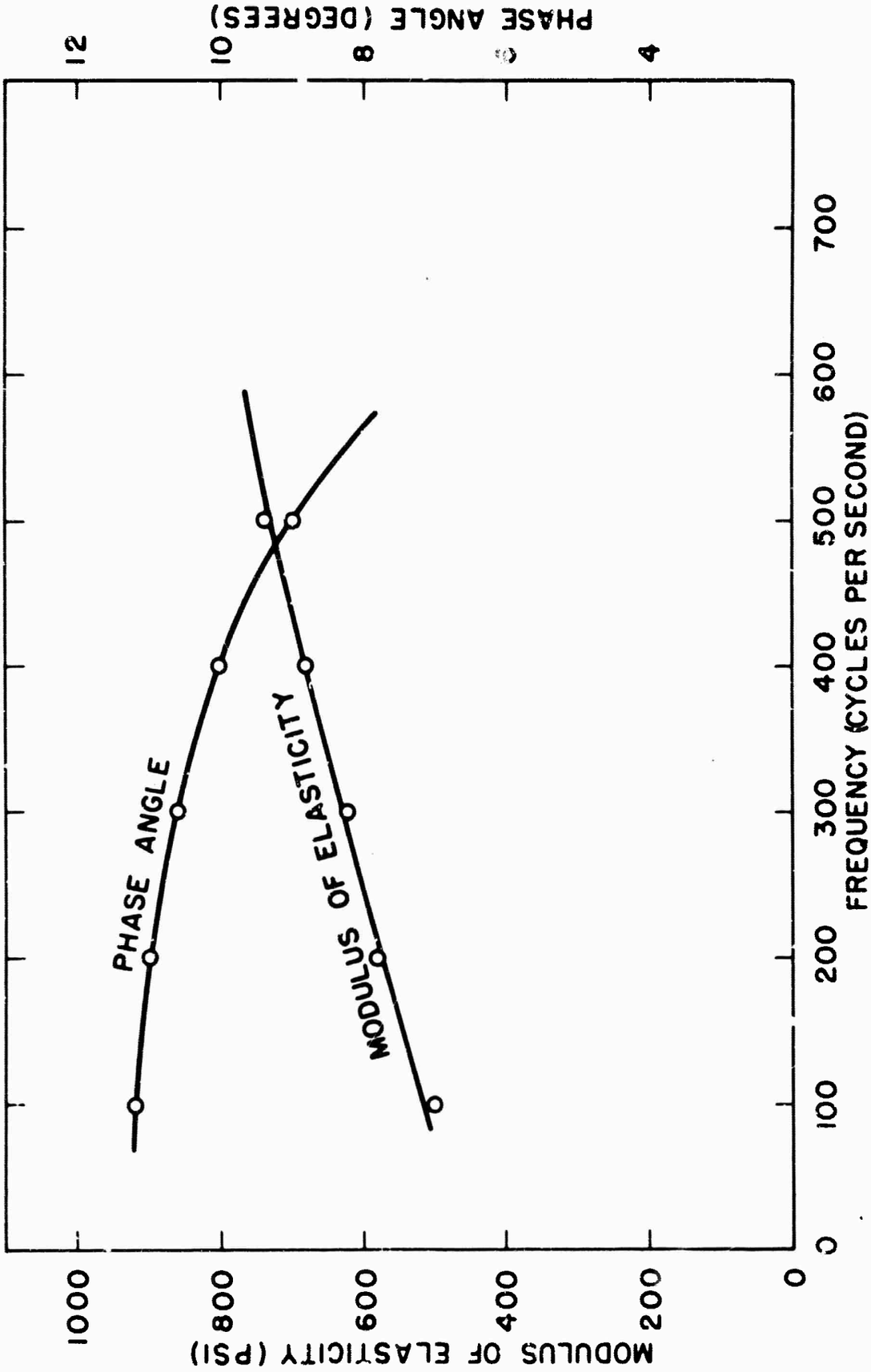

FIG. 24 MODULUS OF ELASTICITY OF HYSOL 4485 AS A FUNCTION OF FREQUENCY OF LOADING

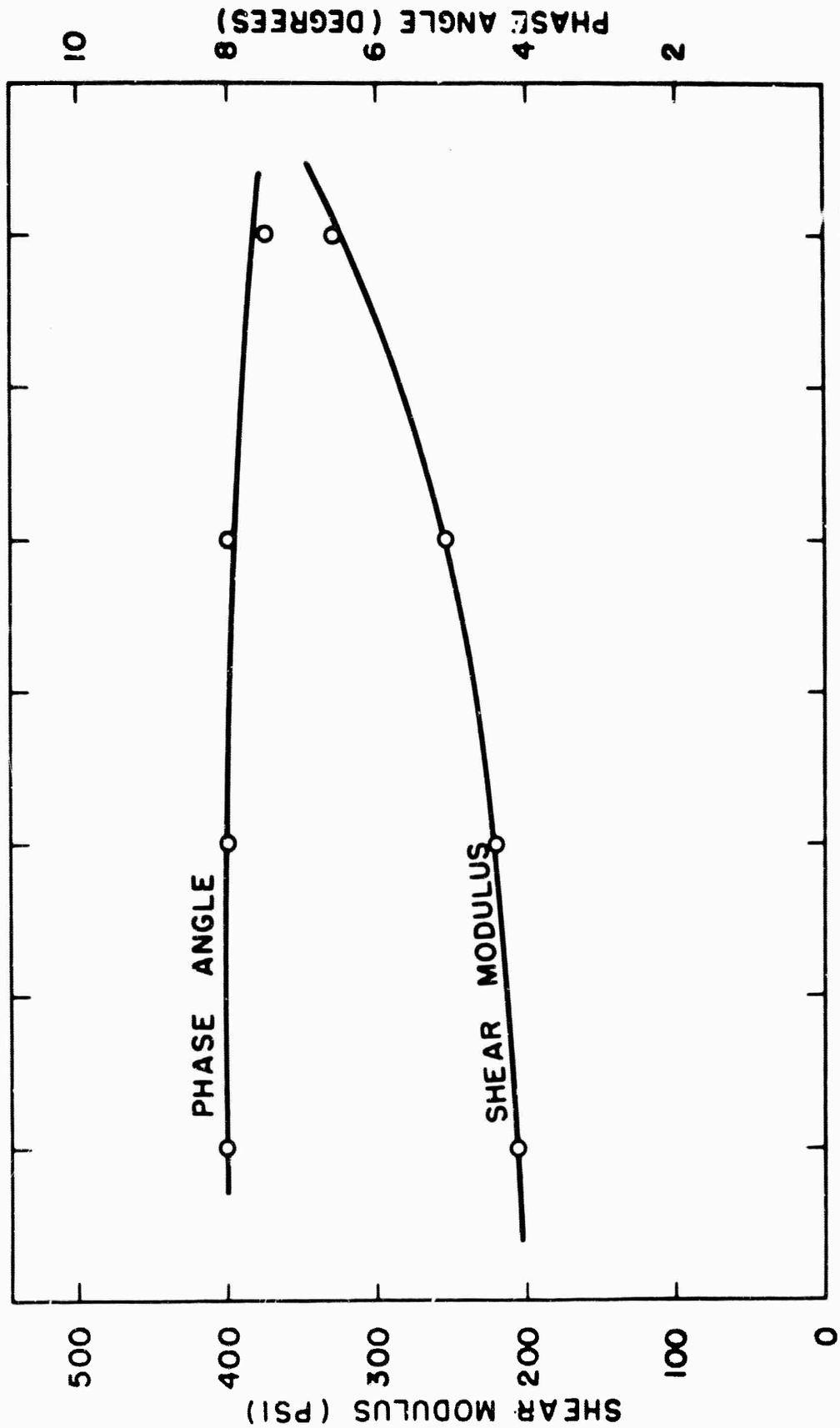

FIG. 25 SHEAR MODULUS OF HYSOL 4485 AS A FUNCTION OF FREQUENCY OF LOADING

Table I

DATA FOR STATIC PHOTOELASTIC STRESS FRINGE VALUE DETERMINATION

Load	Fringe Order	$\frac{4P}{\pi D}$
1 lb	0.97	0.41
2 lb	1.83	0.82
3 lb	2.67	1.23
4 lb	3.48	1.64
5 lb	4.31	2.05
6 lb	5.13	2.46
7 lb	6.09	2.86

Table II

CREEP DATA FOR 20 PSI STUDY

Time After Loading (min)	ϵ_x^L (in/in)	ϵ_y^L (in/in)
0.1	0.0176	0.0392
0.3	0.0180	0.0392
0.5	0.0179	0.0395
0.7	0.0178	0.0401
0.9	0.0183	0.0400
1.0	0.0183	0.0400
2.6	0.0183	0.0402
5.0	0.0183	0.0402
20.0	0.0183	0.0400
37.8	0.0186	0.0403
145.4	0.0198	0.0408
1480.4	0.0199	0.0411

Table III

CREEP DATA FOR 41.7 PSI STUDY

Time After Loading (min)	ϵ_x^L (in/in)	ϵ_y^L (in/in)
0.1	0.0355	0.0738
0.3	0.0357	0.0749
0.5	0.0362	0.0748
0.8	0.0363	0.0748
1.0	0.0363	0.0748
2.0	0.0363	0.0748
5.0	0.0363	0.0748
20.0	0.0363	0.0748
51.5	0.0363	0.0748
188.0	0.0368	0.0750
322.4	0.0368	0.0750
1270.3	0.0373	0.0748

Table IV

VOLTERRA PENDULUM STUDY - V_o = 7.02 in/sec

Time After Impact (millisec)	True Stress (psi)	True Stress (in/in)
1	5.20	0.0080
2	10.54	0.0139
3	15.22	0.0218
4	19.88	0.0266
5	23.52	0.0325
6	27.16	0.0372
7	29.71	0.0420
8	32.14	0.0450
9	33.17	0.0480
10	33.87	0.0488
11	33.33	0.0488
12	32.42	0.0488
13	30.61	0.0470
14	27.90	0.0440
15	24.45	0.0412
16	22.86	0.0374
17	16.18	0.0315
18	12.49	0.0257
19	7.99	0.0208
20	4.22	0.0149
21	0	0.0080

Table V

VOLTERRA PENDULUM STUDY - V_o = 65.5 in/sec

Time After Impact (millisec)	True Stress (psi)	True Strain (in/in)
0.75	32.51	0.039
1.50	85.17	0.113
2.25	117.11	0.174
3.00	154.61	0.231
3.75	186.66	0.293
4.50	225.26	0.357
5.25	258.76	0.412
6.00	281.81	0.457
6.75	296.39	0.494
7.50	301.68	0.518
8.25	299.39	0.524
9.00	286.59	0.518
9.75	269.73	0.494
10.50	231.06	0.463
11.25	207.91	0.418
12.00	174.56	0.371
12.75	141.79	0.314
13.50	105.13	0.262
14.25	73.96	0.207
15.00	51.84	0.139
16.00	0	0.077

Table VI

SINUSOIDAL RESPONSE TESTS-SHEAR MODULUS DETERMINATIONS

Frequency (cycles/sec)	Shear Modulus (psi)	Phase Angle (degress)
100	205	8.0
300	220	8.0
500	255	8.0
700	330	7.5

Table VII

SINUSOIDAL RESPONSE TEST - MODULUS OF ELASTICITY DETERMINATION

Frequency (cycles/sec)	Modulus of Elasticity (psi)	Phase Angle (degree)
100	500	11.2
200	580	11.0
300	625	10.6
400	680	10.0
500	740	9.0

APPENDIX: SUMMARY OF VOLTERRA PENDULUM THEORY

Let $F_1(t)$ be the compressive force produced on the specimen by the impacting pendulum at a time t which is measured from the instant the impacting pendulum contacts the specimen. Let $F_2(t)$ be the force acting on the impacted pendulum. Similarly, let $X_1(t)$ and $X_2(t)$ be the horizontal displacements of the impacting and impacted pendulums respectively measured from their initial positions at the instant $t = 0$. Let M_1 and M_2 be the masses of the impacting and impacted pendulums, respectively.

The change in distance between the two pendulums S(t) is given by:

$$S(t) = X_2(t) - X_1(t) \qquad \text{(Eq. 1)}$$

A double differentiation of Eq. 1 with respect to time gives:

$$\frac{d^2S(t)}{dt^2} = \frac{d^2X_2(t)}{dt^2} - \frac{d^2X_1(t)}{dt^2} \qquad \text{(Eq. 2)}$$

Writing Newton's Second Law of Motion for the impacting and impacted pendulums gives the following relations if the angular movement of the pendulums during impact is small.

$$F_1(t) = M_1 \frac{d^2X_1(t)}{dt^2} \qquad \text{(Eq. 3)}$$

$$F_2(t) = M_2 \frac{d^2X_2(t)}{dt^2} \qquad \text{(Eq. 4)}$$

Solving Eqs. 3 and 4 for $\frac{d^2X_1(t)}{dt^2}$ and $\frac{d^2X_2(t)}{dt^2}$ and substituting these values in Eq. 2 results in:

$$\frac{d^2S(t)}{dt^2} = \frac{F_2(t)}{M_2} - \frac{F_1(t)}{M_1} \qquad \text{(Eq. 5)}$$

Assuming that the time required for the forces acting on both ends of the specimen to become equal is small enough to be neglected, one may write from Newton's Law of Action and Reaction

$$F_2(t) = -F_1(t) \qquad \text{(Eq. 6)}$$

Substitution of Eqs. 6 into 5 gives:

$$\frac{d^2S(t)}{dt^2} = F_2(t)\left[\frac{1}{M_2} + \frac{1}{M_1}\right] \qquad \text{(Eq. 7)}$$

Rearrangement of the terms in Eq. 7 gives the force $F_2(t)$ as a function of specimen acceleration:

$$F_2(t) = \frac{M_1M_2}{M_1 + M_2} \frac{d^2S(t)}{dt^2} \qquad \text{(Eq. 8)}$$

The equation relating the acceleration as measured by the accelerometer $\frac{d^2X_2(t)}{dt^2}$ with the acceleration of the

specimen $\frac{d^2S(t)}{dt^2}$ is found by substituting Eq. 4 into Eq. 7 and simplifying.

$$\frac{d^2S(t)}{dt^2} = \frac{M_1 - M_2}{M_1} \frac{d^2X_2(t)}{dt^2} \qquad \text{(Eq. 9)}$$

Let ℓ (t) be the actual length of the specimen, and then

$$\ell(t) = \ell_o - S(t) \qquad \text{(Eq. 10)}$$

where ℓ_o is the initial length of the specimen and S(t) is the contraction of the specimen obtained by integrating Eq. 9 twice as shown below:

The first integration gives:

$$\frac{dS(t)}{dt} = \frac{M_1 + M_2}{M_1} \int \frac{d^2X_2(t)}{dt^2} dt + C_1 \qquad \text{(Eq. 11)}$$

where $C_1 = U_o$ the velocity of the impacting pendulum at t = 0.

Letting U(t) be the velocity of the impacted pendulum obtained in the first integration, one obtains for the second integration

$$S(t) = \frac{M_1 + M_2}{M_1} \int U(t)\, dt + U_o t + C_2 \qquad \text{(Eq. 12)}$$

where $C_2 = 0$ the contraction of the specimen at t = 0.

If it is assumed that during deformation the volume of the specimen remains constant (since Poisson's ratio is nearly 1/2 for the materials under consideration, this assumption is justified), it is possible to compute the area A(t) from the following relationship:

$$A(t) = \frac{V_o}{\ell(t)} \qquad \text{(Eq. 13)}$$

where V_o is the initial volume of the specimen. Then, in view of Eqs. 13 and 4, the true stress $\sigma(t)$ will be given by:

$$\sigma(t) = \frac{F_2(t)}{A(t)} = \frac{F_2(t)\ell(t)}{V_o} = \frac{M_2 \dfrac{d^2\kappa_2(t)}{dt^2}\ell(t)}{V_o} \qquad \text{(Eq. 14)}$$

And, the true strain by the formula

$$\epsilon(t) = \text{Log}_e \frac{\ell_o}{\ell(t)} \qquad \text{(Eq. 15)}$$

Hence, from equations 14 and 15 the stress and strain can be computed as a function of time and the dynamic stress-strain curves can be drawn.

The material fringe value in stress $f_\sigma(t)$ is given by:

$$f_\sigma(t) = \frac{h\left[\sigma_1(t) - \sigma_2(t)\right]}{2n(t)} \qquad \text{(Eq. 16)}$$

where

h is the thickness of the specimen[1]

$\sigma_1(t)$ and $\sigma_2(t)$ are the principal stresses and their difference is proportional to the maximum shear stress

n(t) is the fringe order at the center section of the specimen.

Since the loading produced by the pendulums is essentially uniaxial σ_2 vanishes and 16 reduces to

$$f_\sigma(t) = \frac{h\,\sigma(t)}{2\,n\,(t)} \qquad \text{(Eq. 17)}$$

The values of $\sigma(t)$ are obtained from Eq. 14 and the values of n(t) are obtained from the Fastax records of the event. For a short interval of time after impact both $\sigma(t)$ and n(t) increase as linear functions of time. Hence, within this interval of time $f_\sigma(t) = f_\sigma$ and moreover

$$f_\sigma = \frac{h\,d\sigma\,(t)/dt}{2\,dn\,(t)/dt} \qquad \text{(Eq. 18)}$$

The primary advantage of expressing f_σ in terms of $\frac{d\sigma}{dt}$ and $\frac{dn}{dt}$ is that the two quantities need not be determined at exactly the same instant since each quantity is constant over the period of time considered.

---

[1] It is assumed here that the thickness, h, of the model does not vary with time after impact. In the interval of time considered in the determination of the material fringe value, this assumption is justified since the time interval is very short. However, if the interval of time were over the entire loading time, h would have to be considered as a function of time.

REFERENCES

1. Becker, H., "Equipment for Watching Propagating Stress Waves", Rev. Sci. Instr., 30, 12, (1959).

2. Thomson, K.C., "Full-field Seismic Modelling", AFCRL-63-685, (1963).

3. Thomson, K.C. and J. A. Hill, "Seismic Model Impacter", AFCRL-63-790, (1963).

4. Baltrukonis, J. H., D. S. Blomquist and E. B. Magrab, "Measurement of the Complex Shear Modulus of a Linearly Viscoelastic Material", The Catholic University of America, Washington, D.C. 20017, Tech. Rep. No. 5 to the National Aeronautics and Space Administration under Research Grant No. NsG-125-61 (Suppl. 3) May 1964.

5. Leaderman, H., "Elastic and Creep Properties of Filamentous Materials", Textile Foundation, Washington, D. C. (1943) p. 175.

6. Ferry, J. D., "Mechanical Properties of Substances of High Molecular Weight VI. Dispersion in Concentrated Polymer Solutions and its Dependence on Temperature and Concentration", J. Amer. Chem. Soc., 72, 3746, (1950).

7. Schwarzl, F. and A. J. Staverman, "Time-Temperature Dependence of Linear Viscoelastic Behavior", J. Appl. Phys., 23, 838, (1952).

8. Tobolsky, A. V. and J. R. McLoughlin, "Elastoviscous Properties of Polyisobutylene V. The Transition Region", J. Polymer Science 8, 543, (1952).

9. Brown, G. W. and D. R. Selway, "Frequency Response of a Photo-Viscoelastic Material", UCRL-7499, Sept. 15, 1963.

10. Volterra, E. and C. S. Barton, "Impact Testing Machine for Rubber-Like Materials", Proc. SESA, 16, 1, (1958), p. 157.